CHALMERS
UNIVERSITY OF TECHNOLOGY

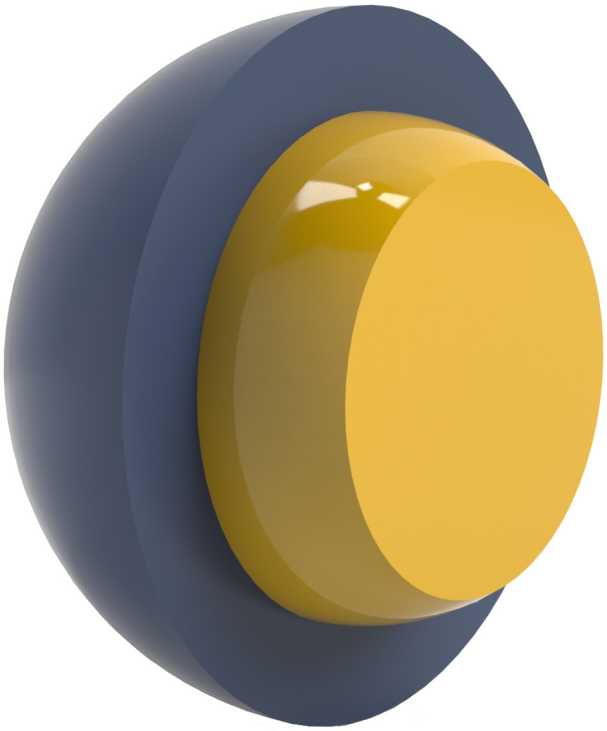

Core-shell particles based on biopolymers and bioactive fatty acids

Encapsulation, characterization and release

Master's thesis in Materials Chemistry

VIKTOR ERIKSSON

Department of Chemistry and Chemical Engineering
CHALMERS UNIVERSITY OF TECHNOLOGY
Gothenburg, Sweden 2019

Master's thesis 2019

Core-shell particles based on biopolymers and bioactive fatty acids

Encapsulation, characterization and release

VIKTOR ERIKSSON

CHALMERS
UNIVERSITY OF TECHNOLOGY

Department of Chemistry and Chemical Engineering
Division of Applied Chemistry
Chalmers University of Technology
Gothenburg, Sweden 2019

Core-shell particles based on biopolymers and bioactive fatty acids
Encapsulation, characterization and release
VIKTOR ERIKSSON

Supervisors: Lars Nordstierna, Chamlmers University of Technology, Department of Chemistry and Chemical Engineering

Markus Andersson Trojer, RISE IVF

Examiner: Lars Nordstierna, Chamlmers University of Technology, Department of Chemistry and Chemical Engineering

Master's Thesis 2019
Department of Chemistry and Chemical Engineering
Division of Applied Chemistry
Chalmers University of Technology
SE-412 96 Gothenburg
Telephone +46 31 772 1000

Cover: A schematic cross sectional image of a core-shell particle with a solid blue polymer shell and a yellow oil core.

Gothenburg, Sweden 2019

Core-shell particles based on biopolymers and bioactive fatty acids
Encapsulation, characterization and release
VIKTOR ERIKSSON
Department of Chemistry and Chemical Engineering
Chalmers University of Technology

Abstract

Through encapsulation of an active substance, a slow and controlled release, rather than instantaneous, can be achieved. This is desired in many applications, with wound care dressings being one of them. To design wound care dressings with a slow release of actives, a feasible approach is to encapsulate the antibacterial substances in microcapsules. The microcapsules can then be incorporated into a non-woven material forming the wound care dressing.

In this project, the microcapsule formulation has been investigated with the goal to produce capsules of higher quality with respect to stability and reduced release rate. Both the shell and core materials of a microcapsule can be altered to achieve this. This gives a substantial freedom in how to produce capsules with the desired properties. Since the microcapsules would be in contact with a wound in the application, biocompatible and biodegradable microcapsules were required. Triglycerides and fatty acid esters were consequently encapsulated in poly(lactic-co-glycolic acid) microcapsules. The fluorophore pyrene was added to the core oil to be able to distinguish the core in fluorescence micrographs and to elucidate the internal structure of the microcapsule. Ethyl cellulose and polycaprolactone have been investigated as alternate shell materials and polyanhydrides have been investigated as plausible shell materials for a fast and triggered release.The release of a model active substance has been investigated for poly(lactic-co-glycolic acid) microcapsules with fatty acid ester and triglyceride cores. By characterizing the size distributions of the microcapsules using two different methods, particle counting by microscopy images has been proven to produce reliable results while still requiring a minimal sample volume.

By using thermodynamical models for interfacial spreading in a three-phase system the morphologies of the final system has been successfully predicted. Using a corresponding thermodynamical approach, a kinetic model was proposed for the formation of core-shell particles via a characteristic intermediate morphology. This kinetic model explained why a core that was shifted to one side and not centered within the microcapsule was observed. Given dichloromethane as volatile solvent, an exceptionally low polymer-water interfacial tension would be required in order to form the most favored intermediate.

Keywords: microcapsule, core-shell particle, internal phase separation method, controlled release, fatty acid ester, triglyceride, poly(lactic-co-glycolic acid)

Acknowledgements

I would like to thank Lars Nordstierna and Markus Andersson Trojer for support thoughout this project. Lars, thank you for the opportunity to perform this master's thesis project. Your help with clever experimental planning has been invaluable. Markus, thank you for your never-ending enthusiasm and encouragement. The intuition and experience regarding microencapsulation that you possess greatly helped me.

I would also like to thank Marina Craig, Alice Flodin, Kristina Hamberg, Petrus Jakobsen and Emil Lukasiewicz from the CapCell project for providing the bigger picture of my work and our discussions during the meetings. Gunnar, Mats, Romain and Szilvia, thank you for all the help regarding experimental equipment. To the rest of the master's thesis workers at Applied Surface Chemistry: thank you for providing an enjoyable working environment.

Lastly, I would like to thank family and friends for your support.

Viktor Eriksson, Gothenburg, June 2019

Contents

List of Figures **xi**

List of Tables **xiii**

1 Introduction **1**
1.1 Purpose and Objectives . . . 2
1.2 Limitations . . . 2

2 Theory **3**
2.1 Internal Phase Separation by Solvent Evaporation . . . 3
2.1.1 Predicting the microcapsule morphology . . . 4
2.1.2 Interfacial tension compartmentalization . . . 4
2.2 Core materials . . . 5
2.2.1 Vegetable oils and triglycerides . . . 6
2.2.2 Fatty acid esters . . . 6
2.2.2.1 Docosahexaenoic acid methyl ester . . . 7
2.2.3 Oxidation of unsaturated fatty acids . . . 7
2.3 Shell materials . . . 8
2.3.1 Poly(lactic-co-glycolic acid) . . . 8
2.3.2 Polycaprolactone . . . 9
2.3.3 Polyanhydrides . . . 9
2.3.4 Ethyl cellulose . . . 10
2.4 Fluorescence in microscopy imaging . . . 10
2.4.1 Pyrene as a fluorescent probe . . . 11
2.5 Microcapsule size distribution . . . 11

3 Methods **13**
3.1 Materials . . . 13
3.2 Microcapsule formulation . . . 13
3.3 Microscopy analysis . . . 15
3.4 Particle size distributions . . . 15
3.4.1 Analysis using microscopy images . . . 15
3.4.2 Analysis using light diffraction . . . 16
3.5 Optical tensiometry . . . 16
3.5.1 Surface energy calculations . . . 17
3.5.2 Interfacial tensions with polymeric dispersants . . . 17

3.6 Release measurements 17
3.6.1 Background subtraction of DHA 18

4 Results and discussion **21**
4.1 Formulation and characterization 21
4.1.1 Size distribution 23
4.1.2 Thermodynamic spreading conditions 25
4.1.3 Capsule stability 26
4.1.4 Alternate shell materials 28
4.2 Optimization for slow release 30
4.2.1 Solid core for lower rate of diffusion 30
4.2.2 Centering of the core 31
4.3 Theory of spreading kinetics 31
4.4 Controlled release of pyrene 34
4.4.1 Effect of microcapsule stability on the release 36

5 Conclusion **39**

Bibliography **41**

A Appendix 1 **I**
A.1 Optical tensiometry I

List of Figures

2.1 Three different morphologies for two-phase particles: a) cross-section of core-shell particle, b) "acorn" particle, c) droplet separation. 3
2.2 Molecular structure of glyceryl trioctanoate. 6
2.3 Molecular structure of the fatty acid ester ethyl linoleate. 6
2.4 Molecular structure of BHT. 7
2.5 Molecular structure of poly(lactic-co-glycolic acid). 8
2.6 Molecular structure of polycaprolactone. 9
2.7 Structure of a polyanhydrides containing either a) aliphatic or b) aromatic segments. 9
2.8 Structure of ethyl cellulose. Depending on the degree of substitution, the R-group ratio of H to C_2H_5 can differ. 10
2.9 Perrin-Jablonski diagram illustrating the process of fluorescence. . . . 10
2.10 Molecular structure of pyrene. 11

3.1 Schematic representation of the microcapsule formulation method. An oil-in-water emulsion is formed by high-speed shearing. The emulsion is diluted with more water phase and the volatile solvent is allowed to evaporate under magnetic stirring to produce microcapsules. 14
3.2 Absorbance spectrum of pyrene in 6 wt% Brij® L23 solution. 18
3.3 UV-vis absorption spectrum for release measurements from microcapsules with DHA methyl ester as core material. The raw sample data ($\cdot\ \cdot\ \cdot$), a blank sample with DHA dissolved in Brij® L23 (- - -) and the filtered spectrum (—) is presented. 19

4.1 Optical microscopy image illustrating the structure of prepared core-shell microcapsules. 21
4.2 Fluorescence microscopy image displaying core-shell PLGA microcapsules with an ethyl linoleate core and $m_s/m_c = 3.1$. The magnification in the inset illustrates the shifted core-shell morphology. 22
4.3 Fluorescence microscopy image displaying the droplet separation present for the combination of PLGA and glyceryl tributanoate. 23
4.4 Number averaged histogram obtained from microscopy images for PLGA microcapsules with $m_s/m_c = 3$ and ethyl linoleate cores along with a log-normal size distribution fitting of the data. 24

4.5 Histogram in Figure 4.4 recalculated to a volume average (●) compared to the volume averaged histogram obtained from light scattering(▲). Both data sets are fitted with log-normal size distribution functions. 24
4.6 Morphology of prepared microcapsules a) directly after formulation and b) after one week of storage under gentle magnetic stirring. . . . 27
4.7 PLGA with a molecular weight of 100 kDa and ethyl linoleate cores a) directly after formulation and b) after one week of storage under gentle magnetic stirring. 28
4.8 Ethyl cellulose microcapsules with ethyl linoleate cores and $m_s/m_c = 0.7$ imaged using a) fluorescence microscopy and b) optical microscopy. 28
4.9 Fluorescence microscopy image of PCL microcapsules with glyceryl trioctanoate as the oil phase. In the inset, an optical micrograph of the rough surface structure of the capsules can be seen. 29
4.10 Polarized light microscopy image illustrating large birefringent fragments of poly(sebacic anhydride). 29
4.11 PLGA microcapsules with ethyl stearate cores visualized with a) fluorescence microscopy and b) optical microscopy using a DIC-filter. . . 30
4.12 Fluorescence microscopy image of the acorn morphology obtained when adding Berol 533 to the core oil. 31
4.13 The kinetic process of internal phase separation. Three different intermediates are possible when going from a DCM droplet to a core-shell particle. In a) the polymer spreads around the DCM-oil droplet, in b) an acorn structure is formed between DCM-oil and polymer and in c) the DCM-oil spreads around the polymer. 32
4.14 Acorn particles observed for PLGA and perfluorooctane. 34
4.15 Fractional release from PLGA microcapsules with $m_s/m_c = 3$ as a function of time. 35
4.16 Fractional release from PLGA microcapsules with $m_s/m_c = 3$ as a function of time. 36
4.17 Fractional release as a function of time for PCL and two molecular weights of PLGA. The core oil was glyceryl trioctanoate for all measurements and $m_s/m_c = 3$. 36
4.18 Fractional release from PLGA microcapsules with ethyl linoleate cores prepared freshly before release measurements (■) and after one week of storage (●). 37

A.1 Dynamic interfacial tension of DCM against 1 wt% PVA in water. Four replicates of the measurements were done. I

List of Tables

2.1 Relative occurrence of the fatty acids, expressed using lipid number notation, in olive oil, sunflower oil and jojoba oil [14, 15]. 6

3.1 Added amounts of the different components for the prepared samples. The amount of added active substance is expressed as a fraction of the core oil weight. 14

4.1 Observed morphologies for the tested core oils. All microcapsules had a PLGA shell with m_s/m_c-ratio of 3. 1 wt% PVA was used as dispersant in the water phase. 22
4.2 Mean radii (μ) and standard deviations (σ) for the log-normal fittings from micrographs of PLGA microcapsules with varying core oils. . . . 24
4.3 Calculated surface energy components (γ^{LW}, γ^{+} and γ^{-}) along with the total surface energy γ^{tot}. All values are presented in mN/m. . . . 25
4.4 Interfacial tensions and calculated spreading coefficients for two of the investigated systems of PLGA microcapsules. Indices o and p are the oil and polymer phases respectively, and w is the water phase containing 1 wt% PVA. Interfacial tensions are presented in mN/m. . 26
4.5 Mean radii (μ) and standard deviations (σ) for the log-normal fittings from micrographs of ethyl cellulose and polycaprolactone microcapsules with glyceryl trioctanoate as core oil. 30
4.6 Interfacial tensions and calculated spreading coefficients for two of the investigated systems. The theoretical intermediate system where the oil phase consists of DCM is also included. Indices o and p are the oil and polymer phases respectively, and w is the water phase containing 1 wt% PVA. Interfacial tensions are presented in mN/m. . 33

A.1 Solubility of pyrene in tested core oils. I
A.2 Fitted parameters to equation 3.2 for the interfacial tension between 1 wt% PVA in water against DCM. II
A.3 Surface tension components of the test liquids used for surface characterization of PLGA along with their contact angles on PLGA. Surface tensions are presented in mN/m and contact angles (θ) in degrees. . . II

1

Introduction

With an aging population, chronic diseases such as diabetes are becoming more common. Between 1980 and 2014 the number of people with diabetes has quadrupled, partly due to an increasing population and aging. During the same time span, its global prevalence has increased from 4.7% to 8.5% for adults which implies that there has been an increase in the risk factors associated with diabetes as well [1]. A complication associated with diabetes is chronic wounds such as ulcers on feet or legs. Ulcers in lower extremities are estimated to develop for 15% of the diabetes patients. For the patients developing ulcers on their feet, 14 - 24% will ultimately undergo amputation [2]. In the majority of these hard-to-heal wounds there is a biofilm present which delays or prevents healing [3]. To avoid this, antimicrobial substances can be used in the wound dressings.

One class of such antimicrobial substances is quaternary ammonium compounds (QACs) [4]. By simply impregnating the wound dressings with antimicrobial substances a fast release of the active substance can be achieved. Initially, all the bacteria would ideally be killed, but the sustained protection over time would be inadequate. To achieve a protection over time, the wound dressings have to be replaced frequently. A more convenient approach is encapsulation of the active substance into so-called microcapsules.

By encapsulating the active substance, a slow and controlled release rate can be achieved. This enables the concentration to be kept above the minimum inhibitory concentration* for a longer period of time. Slow release of QACs enables a less frequent change of the wound dressings. The slower release rate is achieved by having the microcapsule shell acting as a diffusion barrier for the active substance dissolved in the core. Since the microcapsules would be in contact with the wound, the need for biocompatible materials as constituents of the microcapsule arise. Both the shell polymer, the core oil and the antimicrobial substance(s) should be biocompatible and biodegradable. The microcapsules would finally be incorporated into a non-woven cellulose material. The microcapsule-functionalized material would then make up one of the layers in a conventional wound dressing.

*The minimum concentration of active substance where bacterial growth is prevented [4].

1.1 Purpose and Objectives

The purpose of the project is to evaluate how the microcapsule formulation can be optimized to produce capsules of higher quality, i.e. with a more desirable morphology, better stability or a different release profile, while still being biocompatible. It is desired to produce microcapsules with a core-shell morphology that exhibit a satisfactory stability in suspension over time. The release of active substances from the capsules should also be of a desired release rate. Most importantly, the release rate should not be higher than what is required to keep the concentration of active substance above the minimum inhibitory concentration. To obtain microcapsules displaying these properties, a screening will be done with respect to different shell and core materials.

Finally, the kinetics of microcapsule formation will be investigated. A deeper understanding of how the microcapsules are formed enables capsules of higher quality with respect to release rate or stability to be designed.

1.2 Limitations

The main focus of the project will be to understand how the capsule quality can be affected by altering the shell and core materials, although a limited selection of different materials and combinations of materials will still have to be done due to the scope of the project. Furthermore, the active substance will be in the form of a fluorophore as a model compound that distributes selectively in the core. This will be done due to the significantly more convenient analysis and characterization of a fluorophore as compared to antimicrobial substances. Hence, active antimicrobial substances such as QACs will not be encapsulated.

Characterization of the microcapsules will only concern capsules in suspension. Consequently, the incorporation of microcapsules into cellulose fibers will not be included in the scope of this thesis project.

The microcapsule formulation methodology will be limited to internal phase separation by solvent evaporation. There are several methods available for producing microcapsules, including microfluidic emulsification techniques, layer-by-layer assemblies and interfacial polycondensation reactions [5], which consequently will be excluded from the project.

2

Theory

2.1 Internal Phase Separation by Solvent Evaporation

Several techniques for producing microcapsules can be found in the literature. These include interfacial polymerizations, polyelectrolyte multilayer assemblies and internal phase separation by solvent evaporation among others [5–8]. Furthermore, the emulsions required for the interfacial polymerization and internal phase separation methods can be prepared either by microfluidic methods or by high-speed shearing [5, 8, 9]. Preparation of microcapsules following internal phase separation by solvent evaporation is described by Loxley and Vincent [8]. This method has achieved popularity due to its simplicity, only relying on the physical phase separation rather than any chemical reactions. The principle behind this method is based on creating an oil-in-water emulsion in which the emulsion droplets subsequently form the core-shell particles. This is achieved by creating an oil phase consisting of two different solvents together with a polymer and optionally a dye or other active substance. One of the solvents should be a good solvent for the polymer and also volatile and slightly water soluble, such as dichloromethane (DCM), and the other should be a bad solvent for the polymer, such as long alkanes, fatty acid esters or triglycerides, but soluble in the first solvent and non-volatile. Furthermore, both the polymer and the second oil must be water insoluble so that they stay in the emulsion droplets.

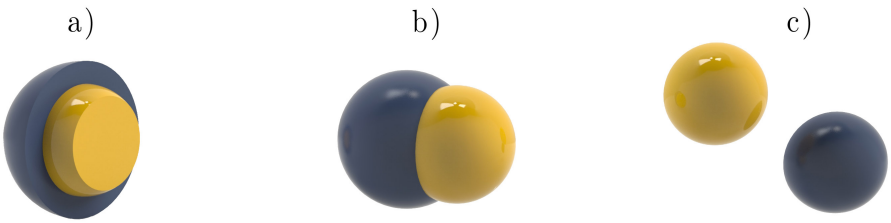

Figure 2.1: Three different morphologies for two-phase particles: a) cross-section of core-shell particle, b) "acorn" particle, c) droplet separation.

When all these four previously mentioned components are mixed into a single oil phase the polymer, the core oil and the active substance should be molecularly dissolved. After the emulsion has been formed, the volatile solvent is allowed to evaporate from the oil droplets through the surrounding water phase. At a certain point during the evaporation, the polymer and non-volatile oil are no longer soluble and phase separates. The phase separation will follow one of several potential pathways such that the overall surface energy of the system is minimized. Some of the possible morphologies for the shell and core materials of the capsules are presented in Figure 2.1. Producing core-shell particles with a solid shell and a liquid core, as seen in Figure 2.1 a), will be the focus of this project.

2.1.1 Predicting the microcapsule morphology

By expressing spreading coefficients the morphology of the capsules can be predicted. The spreading coefficient for the polymer phase can be determined according to Equation 2.1 where *p, o* and *w* indicate the polymer, oil or water phase respectively and γ_{ij} is the interfacial energy between the phases i and j. Expressions can be achieved for the oil (S_o) and water (S_w) similarly [8].

$$S_p = \gamma_{ow} - (\gamma_{po} + \gamma_{pw}) \tag{2.1}$$

Under the condition $\gamma_{ow} > \gamma_{pw}$ there can be three different combinations of the spreading coefficients, Equations 2.2 - 2.4.

$$S_o < 0; \quad S_w < 0; \quad S_p > 0, \tag{2.2}$$

$$S_o < 0; \quad S_w < 0; \quad S_p < 0, \tag{2.3}$$

$$S_o < 0; \quad S_w > 0; \quad S_p < 0. \tag{2.4}$$

Only when the conditions according to Equation 2.2 are met will the microcapsules adopt a core-shell morphology. If Equation 2.3 is fulfilled, so-called "acorn particles" will be formed and by fulfilling Equation 2.4, two separate droplets will form [8]. No kinetics are included in the description by Vincent and Loxley, but this has to be considered in order to understand the core-shell formation. This is therefore investigated further in this report.

2.1.2 Interfacial tension compartmentalization

The establishment of the spreading conditions above necessitates knowledge of the interfacial tension between polymer and liquid. To determine this, the surface energy

of the polymer has to be known. These values can be experimentally determined by using the formalism established by van Oss and coworkers [10]. By measuring contact angles θ on surface i with several test liquids for which the Lifshitz-van der Waals (γ_i^{LW}) and acid-base interactions (γ_i^+, γ_i^-) are known, the surface energy γ_i can be determined according to Equations 2.5-2.7. The Lifshitz-van der Waals contribution takes dispersive forces into account, and the acid-base interactions include contributions from Lewis acid and base interactions. The Young-Dupré equation, Equation 2.8, is then used to determine the solid-liquid interfacial tension γ_{SL}.

$$\gamma_i = \gamma_i^{LW} + \gamma_i^{AB} \tag{2.5}$$

$$\gamma_i^{AB} = 2\sqrt{\gamma_i^+ \gamma_i^-} \tag{2.6}$$

$$1 + \gamma_L \cos\theta = 2\Big((\gamma_S^{LW}\gamma_L^{LW})^{1/2} + (\gamma_S^+\gamma_L^-)^{1/2} + (\gamma_S^-\gamma_L^+)^{1/2}\Big) \tag{2.7}$$

$$\gamma_S = \gamma_{SL} + \gamma_L \cos\theta \tag{2.8}$$

2.2 Core materials

Traditionally, long and hydophobic alkanes such as dodecane or hexadecane have been used when formulating capsules using internal phase separation by solvent evaporation [8, 11]. According to the spreading conditions in Equation 2.2, a large interfacial tension between oil and water (γ_{ow}) is desired to form core-shell particles. This is more easily fulfilled when using a highly hydrophobic oil phase such as a long-chained alkane. Due to requirements for biocompatibility, bioactive fatty acid esters and triglycerides are investigated instead.

Complicated and long systematic and trivial names of fatty acids can be simplified by a numbering system. As an example, linoleic acid ($C_{18}H_{32}O_2$) can be abbreviated as C18:3(n-6). This indicates that the fatty acid has a chain length of 18 carbon atoms, with three double bonds present [12]. Finally, $n-6$ indicates that the first double bond is on the sixth carbon atom from the terminal end [12]. This notation is used frequently throughout the report.

2.2.1 Vegetable oils and triglycerides

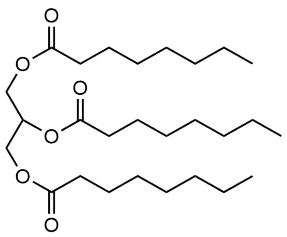

Figure 2.2: Molecular structure of glyceryl trioctanoate.

Vegetable oils are usually found in the form of a triglyceride [12]. Many refined oils contain at least 98% triglycerides, with the rest being diglycerides and free fatty acids [13]. The triglyceride structure includes a glycerol backbone on which three fatty acids are attached through an ester bond. As compared to a synthetic triglyceride, there is usually a distribution of fatty acid chain lengths present in vegetable oils. Commonly, fatty acids ranging from octanoic acid (C8:0) to docosahexaenoic acid (C22:6) can be found in vegetable oils [12].

Table 2.1 shows the relative fractions of fatty acids in olive oil, sunflower oil and jojoba oil [14, 15]. Fatty acids of which the relative fraction is smaller than 1% are excluded from the table. Apart from vegetable oils extracted from plants, synthetic triglycerides are also of interest. One such example is the significantly more short-chained glyceryl trioctanoate.

Table 2.1: Relative occurrence of the fatty acids, expressed using lipid number notation, in olive oil, sunflower oil and jojoba oil [14, 15].

Oil type	16:0 (%)	18:0 (%)	18:1 (%)	18:2 (%)	20:1 (%)	22:1 (%)
Olive oil	10.1	3.0	71.9	7.5	-	-
Sunflower oil	6.2	4.3	20.2	63.2	-	-
Jojoba oil	-	-	12.5	-	67.0	14.5

2.2.2 Fatty acid esters

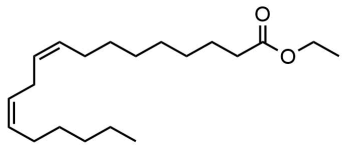

Figure 2.3: Molecular structure of the fatty acid ester ethyl linoleate.

Through transesterification of triglycerides, the glycerol backbone can be replaced with short alkyl groups, typically methyl or ethyl groups. This is the process in which for instance biodiesel is produced from vegetable oil [16]. The molecular structure of a fatty acid ester, ethyl linoleate, is seen in Figure 2.3. Several characteristics such as fatty acid chain length, degree of unsaturation and alkyl chain length can be altered to modify the chemical properties. By altering the degree of unsaturation, the melting point is greatly affected. While ethyl linoleate, seen in Figure 2.3, is liquid at room temperature, the corresponding saturated ethyl stearate is solid at room temperature.

2.2.2.1 Docosahexaenoic acid methyl ester

Among naturally occurring fatty acids, docosahexaenoic acid (DHA) is the longest and most unsaturated with a C22:6 structure [17]. The metabolites from DHA have been found to display anti-inflammatory effects [18]. This makes DHA esters an attractive core substance in microcapsules due to their inherent biological activity.

2.2.3 Oxidation of unsaturated fatty acids

Through a process known as autoxidation, polyunsaturated fatty acids can become peroxidated. This occurs through a radical reaction path that Gardner describes as a three-stage event, reactions 2.a-2.c [19]. Activated singlet oxygen ($^1O_2$) can also oxidize unsaturated fatty acids [20].

$$\mathrm{RH} + \mathrm{X}\cdot \xrightarrow{\text{activation}} \mathrm{R}\cdot + \mathrm{XH} \tag{2.a}$$

$$\begin{aligned} \mathrm{R}\cdot + \mathrm{O_2} &\longrightarrow \mathrm{ROO}\cdot \\ \mathrm{ROO}\cdot + \mathrm{RH} &\longrightarrow \mathrm{ROOH} + \mathrm{R}\cdot \end{aligned} \tag{2.b}$$

$$\left.\begin{aligned} \mathrm{R}\cdot + \mathrm{ROO}\cdot &\longrightarrow \\ 2\,\mathrm{ROO}\cdot &\longrightarrow \\ 2\,\mathrm{R}\cdot &\longrightarrow \end{aligned}\right\} \text{Nonradical products} \tag{2.c}$$

In the initiation step, reaction 2.a, a hydrogen is abstracted at the bis-allylic position of the fatty acid chain. This C-H bond has a bond dissociation energy of 75 kcal/mol [19]. A linear dependence can be seen between the number of bis-allylic methylene groups present in the molecule and the oxidizability [19]. The initiation can be triggered by redox metal ions, ionizing and ultraviolet radiation or photoactivated dyes [21]. In a monounsaturated fatty acid, there are only mono-allylic hydrogen atoms present which have a bond dissociation energy of 88 kcal/mol. Monounsaturated fatty acids are consequently less susceptible to oxidation [19]. As a comparison, the bond dissociation energy of a C-H bond in a saturated carbon chain is approximately 100 kcal/mol [22].

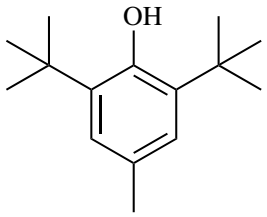

Figure 2.4: Molecular structure of BHT.

Autoxidation of lipids has been found to occur already during emulsification [23]. Due to the large surface area formed during emulsification, this increases the rate of oxidation. Furthermore, the agitation from the homogenizer increases the inclusion of oxygen in the emulsion [23]. An inert nitrogen atmosphere can consequently reduce the oxidation rate. Antioxidants such as butylated hydroxytoluene (BHT), seen

in Figure 2.4, can also be used to prevent the oxidation [24]. The antioxidant properties are achieved by donating hydrogen atoms to the free radicals, so that BHT becomes a radical itself. The aromatic structure, together with the two *tert*-butyl groups stabilizes the BHT radical. BHT is allowed as an additive in food and is generally considered safe at low concentrations [24].

If the autoxidation occurs on polyunsaturated fatty acids, the double bonds shift so that conjugated dienes are created along the fatty acid chain as hydroperoxides form [20]. These hydroperoxides can further react to form for instance malonaldehyde as secondary oxidation products through complex reaction pathways.

2.3 Shell materials

A prerequisite for the shell material in this project is that it is biocompatible and biodegradable. Furthermore, two different classes of shell materials can be imagined. Firstly, there are shells which are relatively stable towards degradation. Capsules composed of these materials in the shell would display a slow release of actives over time. Secondly, shells with materials displaying a much faster triggered degradation are conceivable. This way a rapid and triggered release could be achieved upon exposure to an external stimuli. Such stimuli can be a pH change in the water phase which results in a chemical change in the shell that releases the core substance.

2.3.1 Poly(lactic-co-glycolic acid)

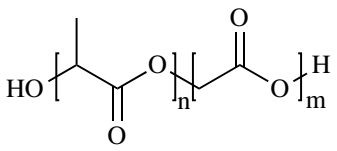

Figure 2.5: Molecular structure of poly(lactic-co-glycolic acid).

Poly(lactic-co-glycolic acid) (PLGA) has received interest in the field of biocompatible and biodegradable polymers [25]. Whereas pure lactic or glycolic acid polymers may be crystalline, the copolymer comprising the two monomers is amorphous. Applications of the polymer ranges from orthopedic implants to drug delivery vehicles [25]. See Figure 2.5 for the molecular structure of the polymer.

The polymer degrades through hydrolysis of the ester linkage in the polymer backbone to form free lactic and glycolic acid [26]. The degradation time is in the order of weeks, dependent on the ratio between the lactic and glycolic acid monomers. By having a more hydrophobic polymer with a higher content of the lactic acid monomer, the degradation time is prolonged [25]. There is also a pH-dependence on the degradation of the polymer [27, 28]. Even at altered pH, the degradation occurs over several days which makes it unfeasible for use as a shell material for triggered release.

2.3.2 Polycaprolactone

Polycaprolactone (PCL) is also a biodegradable polyester. It is semi-crystalline and has a low glass transition temperature and melting temperature of -60 °C and 60 °C, respectively [29]. The molecular structure of the repeating unit in PCL is presented in Figure 2.6. The polymer has received interest when making scaffolds for tissue engineering [30]. Foams, fibers and drug-loaded nanospheres have also been prepared using PCL [29]. Total degradation of PCL happens over 2-4 years depending on molecular weight, which is significantly slower than PLGA.

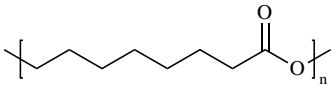

Figure 2.6: Molecular structure of polycaprolactone.

2.3.3 Polyanhydrides

Polyanhydrides are characterized by an anhydride bond in the backbone. This bond is highly reactive towards hydrolysis, especially at alkaline pH [31]. From this, a triggered release could be obtained. The slightly alkaline environment of an inflamed wound therefore further promotes the use of polyanhydrides as triggered release materials [32]. Depending on the structure of the anhydride, the degradation time may vary. Poly(sebacic acid) is an aliphatic anhydride, as seen in Figure 2.7 with the R-group in Figure 2.7a) and $m = 8$, that displays a high crystallinity of 66% [33]. By copolymerizing it with aromatic diacids such as 1,3-bis(p-carboxyphenoxy)propane, having the R-group in Figure 2.7b), the degree of crystallinity can be substantially decreased [33]. Degradation within days or weeks can be observed for aliphatic anhydrides, such as poly(adipic anhydride) or poly(sebacic anhydride) [34, 35]. Anhydrides with aromatic segments, such as poly(1,3-bis(p-carboxyphenoxy)propane), degrade in the time span of months to years [34].

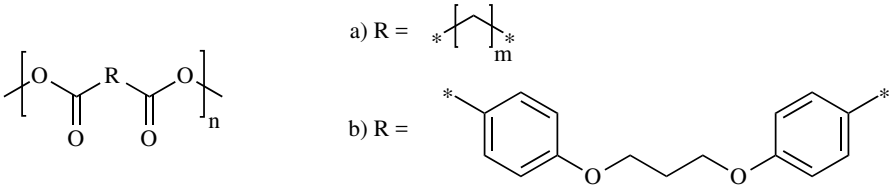

Figure 2.7: Structure of a polyanhydrides containing either a) aliphatic or b) aromatic segments.

2.3.4 Ethyl cellulose

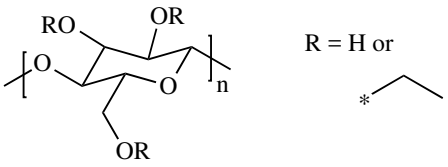

Figure 2.8: Structure of ethyl cellulose. Depending on the degree of substitution, the R-group ratio of H to C_2H_5 can differ.

Ethyl cellulose is a derivative of cellulose, see Figure 2.8. It is available at different degrees of substitution, which affects the properties of the material. Ethyl cellulose has been used for controlled release in pharmaceutical applications, both as a coating on microspheres and as the actual matrix in a microsphere [36, 37]. Proposed core-shell particles have been prepared with ethyl cellulose and plant oils as core material [38]. These core-shell particles were found to have a porous shell of ethyl cellulose with the oil phase contained within it. At the same time, ethyl cellulose is proposed to form oleogels with vegetable oils [39].

2.4 Fluorescence in microscopy imaging

Fluorescence microscopy can be used as a way of distinguishing the microcapsule core from the shell due to intense color at a specific excitation wavelength. The fluorescence process can be illustrated by a Perrin-Jablonski diagram, Figure 2.9. The first stage is absorption of a photon, which excites the fluorophore from the fundamental electronic state S_0 to an excited singlet state, S_2 in Figure 2.9. There are several vibrational energy levels to each electronic state [40]. Secondly, there is an internal conversion which is a nonradiative conversion between two singlet electronic states. Finally fluorescence occurs as a photon of lower energy than the absorbed photon is emitted during relaxation from S_1 to S_0 [40].

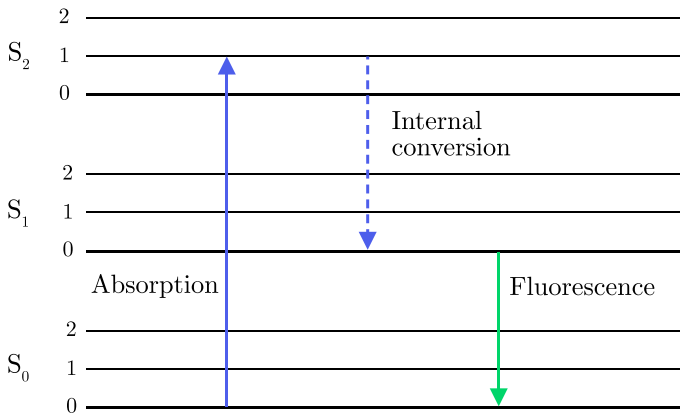

Figure 2.9: Perrin-Jablonski diagram illustrating the process of fluorescence.

2.4.1 Pyrene as a fluorescent probe

Organic fluorophores typically contain aromatic groups with delocalized π-systems [40]. One example of an organic fluorophore is pyrene which is commonly used as a fluorescent probe. The molecule is strongly fluorescent and exhibits several emission peaks in the near-UV region (300-400 nm). A highly hydrophobic molecular structure ensures a low migration into the water phase, lowering background noise in the fluorescence imaging. Due to the hydrophobicity of the molecule, it can be used to, for instance, identify self-association by hydrophobic interactions [41].

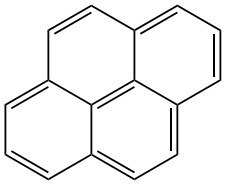

Figure 2.10: Molecular structure of pyrene.

Furthermore, pyrene molecules can form complexes at sufficiently high concentrations [42]. This is called excimer formation, as an abbreviation of excited state dimer. The emission spectrum is unstructured and shifted towards longer wavelengths. Birks summerizes the process of excimer formation in three steps, reactions 2.d-2.f [42].

$$^1\mathrm{M}^* \longrightarrow {}^1\mathrm{M} + h\nu_\mathrm{M} \tag{2.d}$$

$$^1\mathrm{M}^* + {}^1\mathrm{M} \rightleftharpoons {}^1\mathrm{D}^* \tag{2.e}$$

$$^1\mathrm{D}^* \longrightarrow {}^1\mathrm{M} + {}^1\mathrm{M} + h\nu_\mathrm{D} \tag{2.f}$$

Here, ^{1}M and ^{1}M* are the ground state and excited state respectively of the monomer, ^{1}D* is the excimer and $h\nu_\mathrm{M}$ and $h\nu_\mathrm{D}$ are the fluorescence emissions of the monomer and excimer respectively. Fluorescence by the monomer, reaction 2.d, is self-quenched at sufficiently high concentrations of pyrene. This self-quenching is a result of the interaction between ^{1}M* and ^{1}M, reaction 2.e. Finally, the excimer is dissociated in the ground state, reaction 2.f [42]. This can be used in membranes for example, to estimate lateral lipid diffusion where the pyrene is covalently attached to the lipid [43].

2.5 Microcapsule size distribution

The size distribution of microcapsules in a sample prepared by the solvent evaporation method is dependent on the size distribution of the prepared emulsion prior to solvent evaporation. Emulsion droplet size has been found to follow a log-normal size distribution for a variety of systems [44]. It is therefore assumed that the size distribution of produced microcapsules also follow a log-normal size distribution, according to Equation 2.9, where M and S are the mean and standard deviation

of $\ln r$ [11]. The mean and standard deviation of the non-logarithmized r can be expressed as μ and σ respectively, as seen in Equations 2.10 and 2.11.

$$p(r) = \frac{1}{\sqrt{2\pi}Sr} \exp\left(- \frac{(\ln r - M)^2}{2S^2} \right) \qquad r > 0 \tag{2.9}$$

$$\mu = \exp\left(M + \frac{S^2}{2} \right) \tag{2.10}$$

$$\sigma^2 = \left(\exp\left(S^2\right) - 1 \right) \exp\left(2M + S^2\right) \tag{2.11}$$

3

Methods

3.1 Materials

During the project acetone ($\geq$ 99.8%, VWR Chemicals), Brij® L23 (Sigma-Aldrich), Berol 533 (Akzo Nobel), butylated hydroxytoluene (99%, Acros Organics), chloroform ($\geq$ 99.5%, Sigma-Aldrich), dichloromethane (Sigma-Aldrich), diiodomethane (99%, Sigma-Aldrich), glycerol (99%, Sigma-Aldrich), poly(methyl methacrylate)-block-poly(sodium methacrylate) (M_n 600-b-4600 g/mol, Polymersource), poly(vinyl alcohol) (95% hydrolyzed, M_w 95 000 g/mol, Acros Organics) and pyrene ($\geq$ 99.0%, Sigma-Aldrich) was used as received. Milli-Q® water (18.2 MΩ cm, Millipore) was used throughout the project.

The selected oil phases were docosahexaenoic acid methyl ester ($\geq$ 98%, Cayman Chemical), ethyl linoleate ($\geq$ 99%, Sigma-Aldrich), ethyl stearate ($\geq$ 97%, Sigma-Aldrich), glyceryl tributyrate ($\geq$ 99%, Sigma-Aldrich), glyceryl trilinoleate ($\geq$ 95%, TCI Chemicals), glyceryl trioctanoate ($\geq$ 99%, Sigma-Aldrich), glyceryl trioleate ($\geq$ 97.0%, Sigma-Aldrich), hexadecane (99%, Acros Organics), jojoba oil (Sigma-Aldrich), methyl linoleate ($\geq$ 98%, Cayman Chemical), methyl octanoate (99%, SAFC), olive oil (Fluka), perfluorooctane (98%, Sigma-Aldrich) and sunflower oil (Sigma-Aldrich).

The shell materials used were ethyl cellulose (46 cP, 48% ethoxyl, Sigma-Aldrich), polycaprolactone (average M_w 69 000 g/mol, Sigma-Aldrich), poly(D,L-lactide-co-glycolide) (M_w 10 000 g/mol, Polysciences, Inc.), poly(D,L-lactide-co-glycolide) (M_w 97 000 g/mol, Polysciences, Inc.), poly(methyl methacrylate) (M_w 350 000 g/mol, Sigma-Aldrich) and poly(sebacic acid) (Sigma-Aldrich).

3.2 Microcapsule formulation

When creating the emulsion, a *Silent Crusher model M* homogenizer equipped with tool 6F (Heidolph Instruments, Germany) was used. The emulsification was done

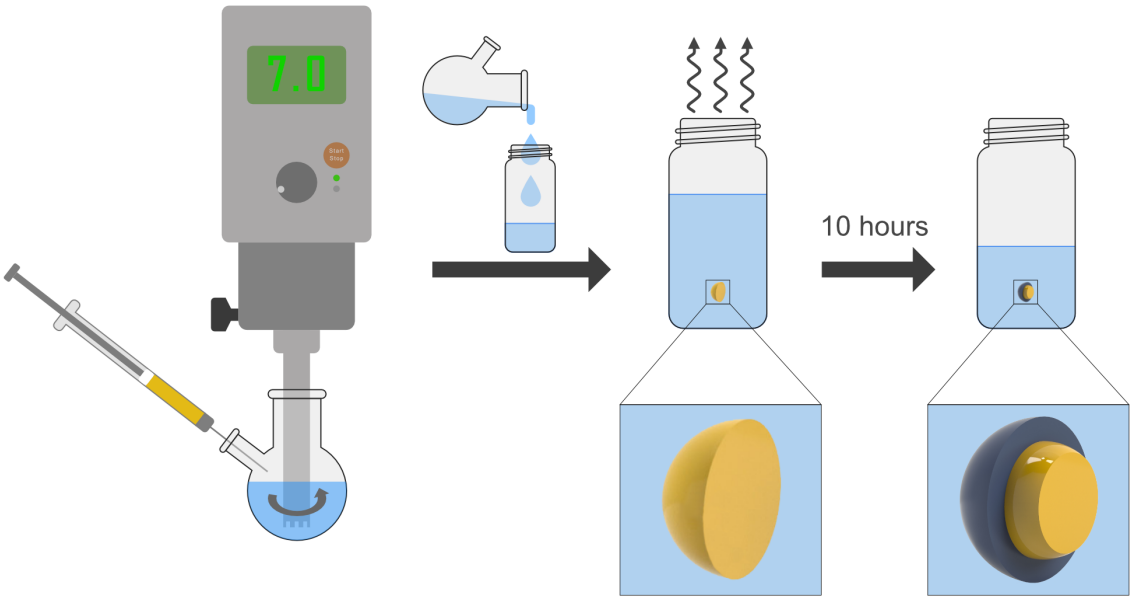

Figure 3.1: Schematic representation of the microcapsule formulation method. An oil-in-water emulsion is formed by high-speed shearing. The emulsion is diluted with more water phase and the volatile solvent is allowed to evaporate under magnetic stirring to produce microcapsules.

in a 5 ml round bottom flask with a side neck (Ace glass, USA). For each batch, 2.4 ml of oil phase was added drop wise over roughly two minutes to 3 ml of water phase. Due to poor mixing using the small homogenizer tool, the emulsification was carried out for 80 minutes, as compared to 60 minutes in the original method by Loxley and Vincent [8]. After emulsification, the emulsion was diluted with an additional 3 ml of water phase. Finally, the emulsion was left in a fume hood for at least 10 hours under gentle magnetic stirring for the volatile solvents to evaporate. This yielded a final theoretical microcapsule concentration of 2 wt%. The amounts of added components is presented in Table 3.1. When the m_s/m_c-ratio was altered, core and shell weights were changed so that the total sum was kept constant. A visualization of the formulation methodology is presented in Figure 3.1.

Table 3.1: Added amounts of the different components for the prepared samples. The amount of added active substance is expressed as a fraction of the core oil weight.

m_s/m_c	DCM (g)	Shell material (g)	Core oil (g)	Acetone (µl)	Active substance (% [w/w])
0.7	3.20	0.055	0.078	200	3
3	3.20	0.100	0.032	200	3

For microcapsule formulations with a solid ethyl stearate core, the evaporation process was carried out at 40 °C which was above the melting point of 36 °C. This was done in order to facilitate the formation of a core-shell morphology where the polymer has to spread around the core. To enable this while still achieving a sufficiently long evaporation period, dichloromethane was replaced with chloroform due to its higher boiling point. The investigated polyanhydrides displayed a poor solubility in

chlorinated solvents and were instead dissolved in ethyl acetate at 50 °C. Furthermore, both emulsification and evaporation of the solvent had to be performed at 50 °C to ensure polymer solubility throughout the emulsification. As ethyl acetate is water soluble at 84.2 mg/ml [45], the water phase was saturated with ethyl acetate prior to adding the oil phase during emulsification [46].

In order to be able to visualize the microcapsules using fluorescence microscopy, pyrene was added to the oil phases. The solubility of pyrene in selected oils is presented in Table A.1 in the Appendix. In general, a pyrene concentration of 3 wt% in the oil phase was used to avoid supersaturation. For release measurements, the concentration was increased to 4 wt%.

3.3 Microscopy analysis

For microscopy analysis, an Axio Imager Z2m equipped with an HBO-lamp and filter set 49 for fluorescence imaging (Zeiss, Germany) was used. When analyzing the microcapsules, a combination of microscopy techniques were used. Optical microscopy with brightfield or differential interference contrast (DIC) illumination was used to visualize the surface structure of the microcapsules. Furthermore, fluorescence microscopy was used to attain knowledge regarding the morphology of the core-shell particles. Due to the selective partitioning of pyrene in the core substances, the fluorescence intensity made it possible to differentiate oil from polymer.

3.4 Particle size distributions

For the determination of size distributions, two different techniques were employed. These were particle counting from microscopy images and light diffraction-based measurements. Particle counting from microscopy images gave a number-averaged size distribution, whereas light diffraction methods gave a volume-averaged size distribution. It was therefore necessary to recalculate microscopy size distributions by volume basis in order to compare the two sets of results.

3.4.1 Analysis using microscopy images

Size distributions determined from optical microscopy images were analyzed using ImageJ (National Institutes of Health, USA). Five different images were taken for each batch, or a total of at least 600 microcapsules, in order to reduce the uncertainty. By using thresholds and other image filters, the calculation of the area for each particle could be automated. The area of each capsule was then converted to

a radius, assuming the capsules to be perfect spheres projected onto a 2D surface, which then was plotted and a lognormal fitting was done using Matlab (Mathworks, USA).

By using microscopy images for size distribution determination, a very small sample volume of about 20 µl was required. Furthermore, it was possible to separate flocculated particles or filter out larger aggregates, capsule fragments or free oil droplets from the analysis. This did, however, introduce the risk of a biased result. Results from microscopy analysis were therefore compared to results from light diffraction measurements to ensure a minimal bias.

3.4.2 Analysis using light diffraction

A Mastersizer Microplus (Malvern Panalytical, UK) was used for diffraction-based size distribution determination. Through irradiation of the sample with light from a He-Ne laser ($\lambda = 633$ nm) an array of detectors recorded the scattering of the incoming light as it passed through the sample. The sample size for diffraction analysis was significantly larger as compared to microscopy analysis, around 3 ml. Based on the scattering, theroretical models is used to correlate the scattering to a particle size distribution in the analysis software.

Size distribution analysis by light diffraction is highly sensitive to aggregates in the sample. As large particles are weighted higher due to the volume-based averaging, results showing bimodal peaks may very well in fact be a unimodal distribution with larger aggregates or flocculated particles. Free oil droplets would also affect the apparent size distribution. Care was therefore taken to run diffraction analysis of the samples as soon as possible after capsule formulation.

3.5 Optical tensiometry

To determine the surface tensions, interfacial tensions and contact angles of selected liquids, an Attension Theta optical tensiometer was used. Surface and interfacial tensions could be determined by fitting the droplet shape to the Young-Laplace equation, Equation 3.1, where γ is the surface or interfacial tension, $\Delta\rho$ is the difference in density between droplet and the surrounding phase, g is the gravitational constant, R_0 is the drop apex radius and β is a shape factor.

$$\gamma = \Delta\rho g \frac{R_0^2}{\beta} \tag{3.1}$$

3.5.1 Surface energy calculations

PLGA substrates were prepared by spin coating 22 x 22 mm glass slides with 100 µl of PLGA dissolved in DCM at 1 wt% in a Spin 150 spin coater (SPS-Europe, Netherlands). The samples were spin coated at 600 rpm for 120 s. By measuring the contact angles of diiodomethane, glycerol, hexadecane and water on PLGA substrates the surface energy could be determined. Through use of non-linear regression analysis in Matlab (Mathworks, USA), a fitting to Equation 2.7 could be performed. The solid-liquid interfacial tensions could then be determined from Equation 2.8 using the contact angles of the appropriate liquids. The known surface tensions (γ_L) along with the dispersive Lifshitz-van der Waals (γ_L^{LW}), polar acid (γ_L^+) and base (γ_L^-) components of the test liquids required for the measurements are presented in Table A.3 in the appendix [47].

3.5.2 Interfacial tensions with polymeric dispersants

Due to the slow diffusion of polymeric dispersants, the interfacial tension between two immiscible liquids does not attain its equilibrium value instantaneously. An empirically determined equation for the kinetic dependence of interfacial tension has been proposed by Xi Yuan and Rosen [48]. This can be seen in Equation 3.2. Here $\gamma(t)$, γ_0 and γ_e are the interfacial tensions at time t, initially and at equilibrium, respectively. τ is a relaxation constant and n is a dimensionless constant. By measuring interfacial tensions as a function of time, a fitting to Equation 3.2 could be performed.

$$\frac{\gamma(t) - \gamma_e}{\gamma_0 - \gamma_e} = \frac{1}{1 + (t/\tau)^n} \tag{3.2}$$

3.6 Release measurements

For release measurements, 2 ml of prepared microcapsule suspension was added to 198 ml 6 wt% Brij® L23 solution. This is a nonionic surfactant that helps to increase the solubility of pyrene in the continuous phase by solubilizing it in micelles. At given times, an aliquot of approximately 4 ml was taken from the release suspension and immediately filtered through a Pall Acrodisc® 25 mm syringe filter with a 0.2 µm Fluorodyne® II membrane [49, 50]. The selection of membrane material is important to ensure that as little as possible of the analyte adsorbs to the membrane itself [51]. After filtration, the filtrate was hence free from microcapsules which allowed for detection of pyrene in only the continuous phase at the given time of filtration.

Following filtration, the concentration of pyrene was determined using an Agilent 8453 UV-vis spectrophotometer. By expressing the Beer-Lambert law, Equation

3.3, a linear relationship between absorbance and concentration was obtained.

$$A = \varepsilon c l \tag{3.3}$$

A is the absorbance in the sample calculated as $A = -\log_{10}(I_1/I_0)$ with I_0 and I_1 being the initial light intensity and light intensity after passing the sample, respectively. ε is the molar absorptivity coefficient, c is the concentration of studied analyte in solution and l is the path length through the cuvette.

The ratio between microcapsule suspension and surfactant solution was chosen to yield a maximum absorption within the linear range of the calibration curve for pyrene. Linearity was obtained up to 2.5 mg/l [50]. Absorbance measurements were performed at the maximum absorbance wavelength 242 nm. To obtain the total loading of the microcapsules (m_{tot}), 2 ml of the release suspension was diluted with 6 ml ethanol. This shifted the pyrene equilibrium completely towards the continuous phase. After allowing all of the pyrene to leach out of the microcapsules into the ethanol solution, an aliquot was filtered and the UV-absorbance was measured. See Figure 3.2 for the absorbance spectrum of pyrene in Brij® L23 solution. Since the absorbance was measured in the UV range, Hellma Analytics Suprasil® quartz cuvettes were used to avoid interferrence from the cuvette material on the absorbance.

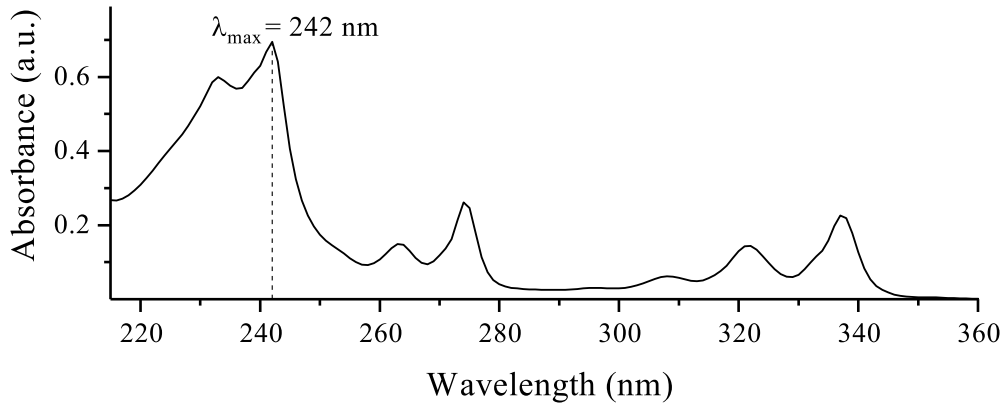

Figure 3.2: Absorbance spectrum of pyrene in 6 wt% Brij® L23 solution.

3.6.1 Background subtraction of DHA

When performing release measurements from microcapsules with the methyl ester of DHA as core material, an absorption band from the oil could be observed apart from the distinct peaks of pyrene. This is presented in Figure 3.3. Due to the high signal intensity at 242 nm, the samples had to be diluted with equal parts of 6% Brij® L23 solution. The absorbance was recalculated to account for dilution in post-

processing which allowed comparison of the three spectra. By introducing a blank sample containing the DHA methyl ester dissolved in Brij® L23, a subtraction of the blank from the raw release spectrum could be performed. This way, only the contribution to the absorbance from pyrene was measured.

Absorbance corresponding to the oil phase was only seen for the methyl ester of DHA, and not the other investigated core oils. It was thought to originate from the oxidation products of DHA, as this absorbance only could be detected after storage of the DHA-containing blank sample for roughly one week. Through formation of conjugated dienes along the fatty acid chain, UV absorption would be seen to increase. Secondary oxidation products such as malonaldehyde could also cause absorption in the UV region. Since the DHA fatty acid contains a total of six double bonds, the expected abundances of diene groups or secondary oxidation products are significantly higher in DHA as compared to for example linoleic acid which only contain two double bonds. Furthermore, as the oxidation rate increases with increasing number of double bonds in the fatty acid, the UV absorbance would increase more rapidly in DHA as compared to other less unsaturated fatty acids.

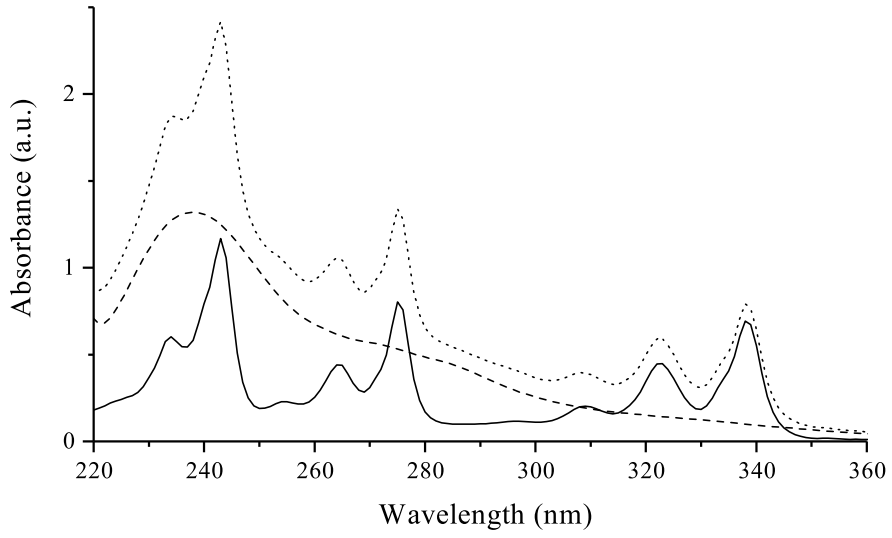

Figure 3.3: UV-vis absorption spectrum for release measurements from microcapsules with DHA methyl ester as core material. The raw sample data (· · ·), a blank sample with DHA dissolved in Brij® L23 (- - -) and the filtered spectrum (—) is presented.

4

Results and discussion

Two distinct sets of results are presented here: those related to the formulation and characterization of microcapsules and those related to the release of actives from formulated microcapsules. Morphologies and size distributions of the microcapsules were characterized prior to investigating their release properties. Furthermore, a theoretical framework for the kinetics of internal phase separation is discussed in order to attempt to alter the formulation produce microcapsules of higher quality. This included capsules with an improved stability or capsules displaying a more beneficial release profile.

4.1 Formulation and characterization

Initially, a screening was performed to evaluate which oil phases could be used to produce core-shell microcapsules. A representative optical microscopy image of PLGA microcapsules with ethyl linoleate cores and $m_s/m_c = 3$ illustrating the observed capsule structure is presented in Figure 4.1. Table 4.1 presents the obtained morphology for all tested core oils. For all of the systems, PLGA was used as a shell material with $m_s/m_c = 3$ and pyrene was the chosen active substance. Core-shell microcapsules were produced for a large variety of oils. This included the highly unsaturated and bioactive docosahexaenoic acid methyl ester as well as saturated oils of shorter chain lengths as glyceryl trioctanoate. It was therefore clear that the investigated microcapsule system with PLGA as shell material allowed for a versatile

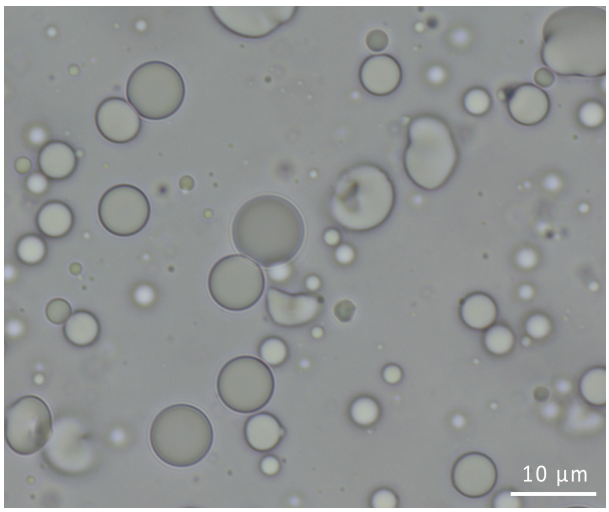

Figure 4.1: Optical microscopy image illustrating the structure of prepared core-shell microcapsules.

selection of biocompatible core oils.

Table 4.1: Observed morphologies for the tested core oils. All microcapsules had a PLGA shell with m_s/m_c-ratio of 3. 1 wt% PVA was used as dispersant in the water phase.

Core oil	Morphology
DHA methyl ester	Core-shell
Ethyl linoleate	Core-shell
Ethyl stearate	Core-shell
Glyceryl tributyrate	Droplet separation
Glyceryl trioleate	Core-shell
Glyceryl trilinoleate	Core-shell
Glyceryl trioctanoate	Core-shell
Jojoba oil	Core-shell
Methyl linoleate	Core-shell
Methyl octanoate	Droplet separation
Olive oil	Core-shell
Sunflower oil	Core-shell

A good agreement between the thermodynamical theory of internal phase separation in section 2.1.1 and the observed results was seen. The more hydrophilic core substances glyceryl tributyrate and methyl octanoate did not produce core-shell particles. No limitations on core-shell formation were found for the more hydrophobic and highly unsaturated core oils tested.

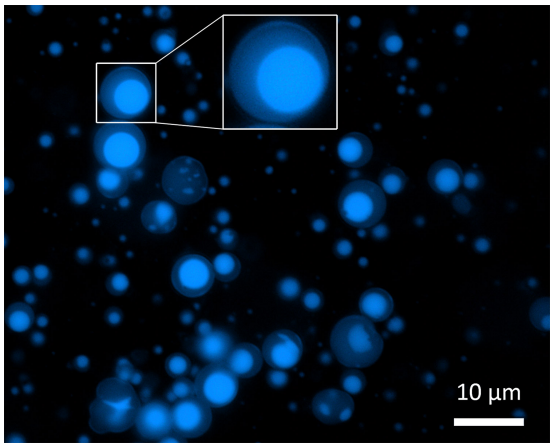

Figure 4.2: Fluorescence microscopy image displaying core-shell PLGA microcapsules with an ethyl linoleate core and $m_s/m_c = 3.1$. The magnification in the inset illustrates the shifted core-shell morphology.

For all microcapsules where a core-shell morphology was obtained, the core was shifted to one side and not centered within the capsule. Using fluorescence microscopy, this could be visualized with the hydrophobic dye pyrene added to the oil phase. As PLGA was more hydrophilic than the core oil, Figure 4.2 illustrates the selectively dyed core of the microcapsule, with the fluorescence intensity being significantly lower in the shell. From an applied perspective with the release rate or stability in mind, a centered core would be more beneficial than the shifted core. When increasing the m_s/m_c-ratio to five, capsules with multiple cores could be observed, probably due to the difficulties of an increased polymer fraction to spread around a single core.

Two of the PLGA microcapsule formulations did not display a core-shell morphology. Figure 4.3 displays the morphology for the combination of PLGA and glyceryl tributyrate. A uniform fluorescence intensity throughout the spheres suggested that they in fact were homogeneous spheres. Apart from the spheres, large coalesced oil domains could be observed in the sample, suggesting that there was a droplet separation between shell and core. For the combination of PLGA and methyl octanoate, similar apparently homogeneous spheres could be observed, although without the same macroscopic oil domains present.

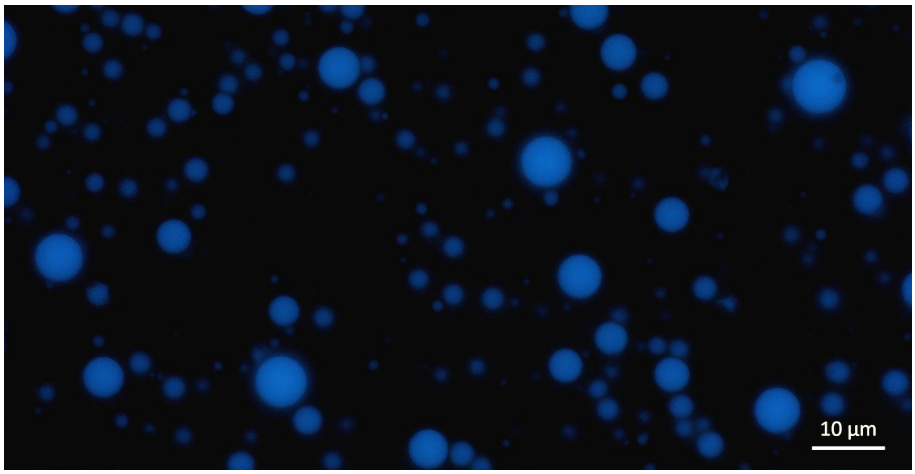

Figure 4.3: Fluorescence microscopy image displaying the droplet separation present for the combination of PLGA and glyceryl tributanoate.

4.1.1 Size distribution

A size distribution determination was only performed on formulations where a core-shell morphology was obtained. The size distribution of microcapsules with ethyl linoleate cores is presented in Figure 4.4. It was possible to get a good fit of the data to the log-normal distribution function, with a R^2 of 0.96. Simiar results were seen for all of the core-shell systems. Fitting parameters μ and σ from the lognormal size distribution function for all prepared microcapsule systems is presented in Table 4.2. The similarities in the results suggested that the core oil influence on capsule size was negligible and that there was a high reproducibility in the formulation process.

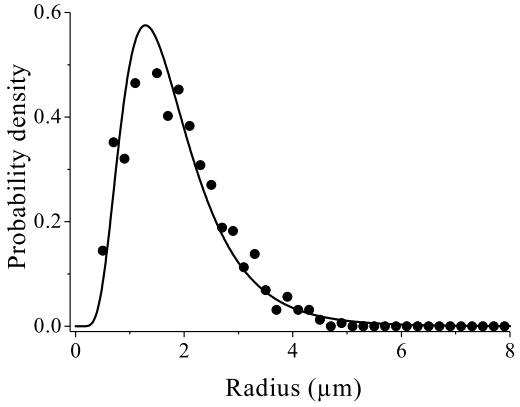

Figure 4.4: Number averaged histogram obtained from microscopy images for PLGA microcapsules with $m_s/m_c = 3$ and ethyl linoleate cores along with a log-normal size distribution fitting of the data.

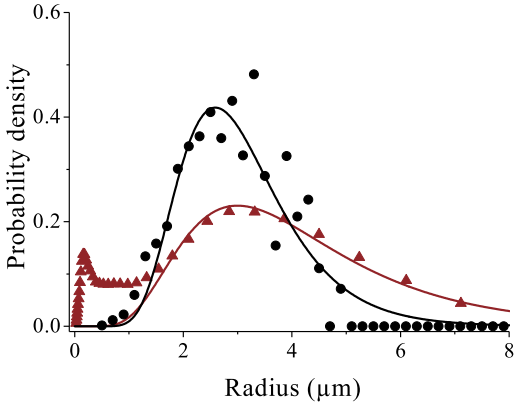

Figure 4.5: Histogram in Figure 4.4 recalculated to a volume average (●) compared to the volume averaged histogram obtained from light scattering(▲). Both data sets are fitted with log-normal size distribution functions.

Table 4.2: Mean radii (μ) and standard deviations (σ) for the log-normal fittings from micrographs of PLGA microcapsules with varying core oils.

Core oil	Mean radius μ (µm)	Standard deviation σ (µm)
DHA methyl ester	1.50 ± 0.06	0.63 ± 0.10
Ethyl linoleate	1.82 ± 0.08	0.86 ± 0.15
Ethyl stearate	1.45 ± 0.05	0.57 ± 0.09
Glyceryl trilinoleate	1.64 ± 0.06	0.66 ± 0.10
Glyceryl trioctanoate	1.26 ± 0.05	0.39 ± 0.06
Glyceryl trioleate	1.45 ± 0.05	0.48 ± 0.07
Jojoba oil	1.46 ± 0.06	0.54 ± 0.09
Methyl linoleate	1.44 ± 0.06	0.68 ± 0.12
Olive oil	1.56 ± 0.06	0.71 ± 0.11
Sunflower oil	1.63 ± 0.20	2.26 ± 0.83

In Figure 4.5 the histogram from Figure 4.4 was recalculated to a volume average after which a new log-normal fitting was performed. This was finally compared to the histogram from light scattering. Although artefacts were introduced to the microscopy histogram due to the re-scaling from number average to volume average, a good agreement between the two analysis methods was observed. The histogram obtained from light scattering displayed a secondary peak at 0.2 µm. This was most likely not an actual bimodal size distribution, but rather error from the analysis due to capsule fragments or other minor impurities in the sample. Hence, this data was filtered out prior to performing the fitting of the size distribution function. For the volume-averaged histogram obtained from microscopy, no particles with radii larger than about 5 µm were detected, while the light scattering detected particles with radii of up to 8 µm. This was due to the difference in sample volume. Analyzing around 800 particles in the microscope was sufficient for obtaining a number-averaged size distribution, but not for producing reliable volume-averaged

statistics on the largest particles. Furthermore, as the larger particles were weighted higher for a volume-average this introduced error in the conversion from number average to volume average.

4.1.2 Thermodynamic spreading conditions

To understand the thermodynamics of the core-shell formation, the free surface energy was determined for PLGA. Table 4.3 lists the experimentally determined surface energy components of PLGA. As a comparison, values for poly(methyl methacrylate) (PMMA) were included from Andersson Trojer et al. [11]. A higher Lewis base contribution (γ^-) was seen for PLGA as compared to PMMA, which was reasonable given the increased hydrophilicity and relative oxygen abundance of PLGA.

Table 4.3: Calculated surface energy components (γ^{LW}, γ^+ and γ^-) along with the total surface energy γ^{tot}. All values are presented in mN/m.

Polymer	γ^{LW}	γ^+	γ^-	γ^{tot}
PLGA	32.9	0	16.2	32.9
PMMA [11]	39.5	0	3.65	39.5

Knowing the surface energy of PLGA, the interfacial tensions polymer-oil and polymer-water phase could be determined from contact angles of the oil and water phases on PLGA. The experimental values of the contact angles are presented in Table A.3 in the appendix. After determining the three relevant interfacial tensions oil-water, polymer-oil and polymer-water, spreading coefficients could be calculated and morphologies could be predicted. The interfacial tensions, spreading coefficients, predicted and observed morphologies are presented in Table 4.4.

A core-shell morphology was predicted for capsules with both ethyl linoleate and glyceryl tributyrate cores. For ethyl linoleate the prediction was in accordance with the observed morphology. For glyceryl tributyrate, on the other hand, the observed morphology was a droplet separation. A higher oil-water interfacial tension for ethyl linoleate was driving core-shell formation. The requirement for sufficiently hydrophobic core oils was therefore valid. The more hydrophilic oil had a lower oil-water interfacial tension which with the addition of surface active PVA at the interface led to morphologies that were not desired. It is worth noting that the value of S_p for glyceryl tributyrate was close to zero. An acorn prediction was therefore possible within the experimental error. To predict the observed droplet separation morphology, S_w should be positive. This was far from what was experimentally determined. It could therefore be that the glyceryl tributyrate was soluble in PLGA so that the observed morphology in fact was a spherical matrix of glyceryl tributyrate dissolved in PLGA. This way a spherical, seemingly homogeneous sphere would be observed in the microscope. If a higher solubility in the polymer was observed when residual amounts of DCM still was remaining, the oil domains that phase separated

from the microcapsules could be explained.

Table 4.4: Interfacial tensions and calculated spreading coefficients for two of the investigated systems of PLGA microcapsules. Indices o and p are the oil and polymer phases respectively, and w is the water phase containing 1 wt% PVA. Interfacial tensions are presented in mN/m.

							Morphology	
Oil phase	γ_{ow}	γ_{po}	γ_{pw}	S_o	S_w	S_p	Predicted	Observed
Ethyl linoleate	21.20	3.87	11.05	-14.02	-28.38	6.29	Core-shell	Core-shell
Glyceryl tributyrate	15.56	4.15	11.05	-8.66	-22.46	0.37	Core-shell	Droplet separation*

4.1.3 Capsule stability

The prepared PLGA microcapsules displayed good initial colloidal stability. After storage under gentle magnetic stirring at room temperature for a few days, the capsules could be seen to start breaking and releasing the core oil. Figure 4.6 illustrates the process evolution of prepared microcapsules over time. After storage, changes in the core structure of the microcapsules could be observed. As the fluorescence intensity became constant across the entire microcapsule, it indicated that the oil phase had leaked out of the microcapsules to leave a hollow polymeric shell. Furthermore, the free oil droplets could be observed in a higher focus plane in the microscope sample due to their lower density. Some of the microcapsules revealed a shrunken core, plausibly due to the oil being partially released. Corresponding brightfield images of capsules after one week were identical to those captured initially after formulation, suggesting that no macroscopic degradation of the PLGA was present. The stability was increased when the microcapsules were added to the release bath as compared to being stored in the formulated suspensions. When added to the release bath, the microcapsule suspension was diluted from 2 wt% to 0.02 wt%. It was therefore hypothesized that the microcapsules broke by mechanical abrasion from colliding with each other. As the core was shifted from the center of the microcapsule, the shell became significantly thinner on one side. If a small hole was formed at the thinnest part of the microcapsule, it would allow the core oil to slowly leak out of the capsule over time. In a more dilute suspension, the number of collisions would decrease which could explain the improved stability. Freezing the capsule suspension directly after formulation could possibly be done in order to store the microcapsules over longer periods of time.

*Glyceryl tributyrate was possibly slightly soluble in PLGA.

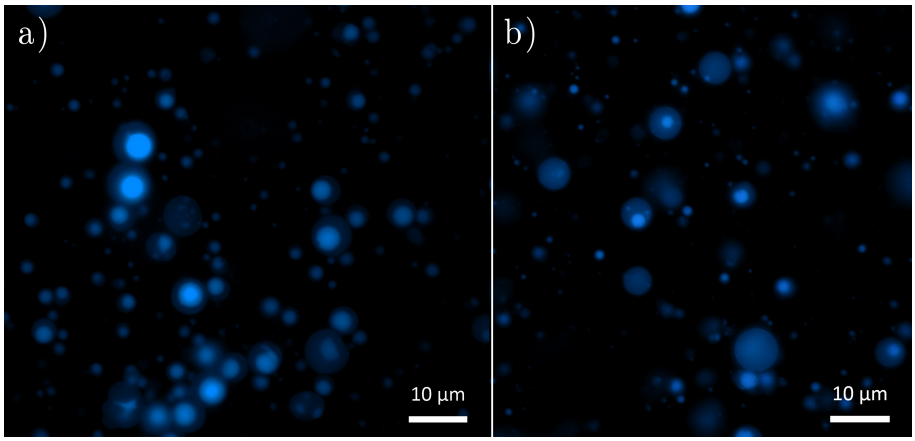

Figure 4.6: Morphology of prepared microcapsules a) directly after formulation and b) after one week of storage under gentle magnetic stirring.

Furthermore, a low oxidative stability of capsules containing unsaturated fatty acid derivatives could be observed. As the oxidation rate increases with an increasing degree of unsaturation, the observed effect was most prominent for capsules containing DHA methyl ester. The deterioration of the microcapsules where the core oil was released into the water phase occurred more rapidly for highly unsaturated oils. As the core oil was oxidized, its chemical properties was affected greatly which led to a faster degradation of the microcapsules and a potential loss of bioactivity in the case of DHA. By adding BHT at 1 wt% of the core oil prior to capsule formulation, the oxidative stability was drastically improved. While the microcapsule suspension changed color from white to amber within a few days to a week as the oil oxidized, no color change could be observed for BHT-treated suspensions. By performing all steps of the formulation from emulsification to solvent evaporation under nitrogen gas as well as storing the samples under nitrogen the oxidation rate was reduced, although not to the same extent as when adding an antioxidant. A complete removal of all oxygen present is difficult, and was probably not achieved.

It was hypothesized that a higher molecular weight of the PLGA would improve the stability over time due to better mechanical properties of the higher molecular weight. This was also what was observed, see Figure 4.7. After one week of storage the majority of the microcapsules were intact, which was a significant improvement. No quantitative measurements on capsule stability were determined, although qualitative comparisons for capsules directly after formulation and after one week of storage can be seen in Figure 4.7.

It was, however, observed that the cores became even more shifted towards one side during formulation as compared to PLGA of lower molecular weight. This was thought to be attributed to higher viscosity and thereby slower kinetics of the PLGA with higher molecular weight. Despite attempts to affect the kinetics of the internal phase separation by reducing the evaporation rate of DCM to almost 24 hours, no differences in core morphology could be observed.

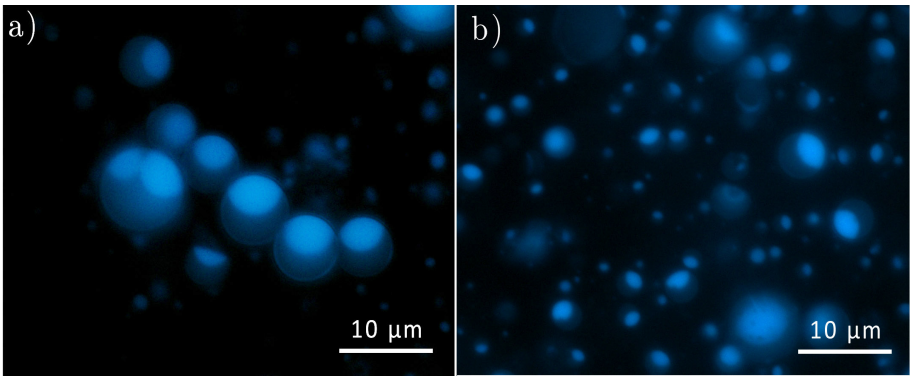

Figure 4.7: PLGA with a molecular weight of 100 kDa and ethyl linoleate cores a) directly after formulation and b) after one week of storage under gentle magnetic stirring.

4.1.4 Alternate shell materials

Ethyl cellulose

Microcapsules with ethyl cellulose as shell material were formulated with both ethyl linoleate and glyceryl trioctanoate as core materials. Due to the high viscosity of dissolved ethyl cellulose in DCM, the m_s/m_c-ratio had to be decreased to 0.7. A fluorescence microscopy image as well as an optical microscopy image of the formulated microcapsules is presented in Figure 4.8. Smooth shells with large indentations could be observed. It was, however, difficult to ascertain whether a core-shell morphology was obtained due to the thin shell. It is also possible that there was formation of an oleogel between ethyl cellulose and the oil phase. Due to the indentations in the surface and the thin shell that had to be used, no release measurements were performed on ethyl cellulose microcapsules.

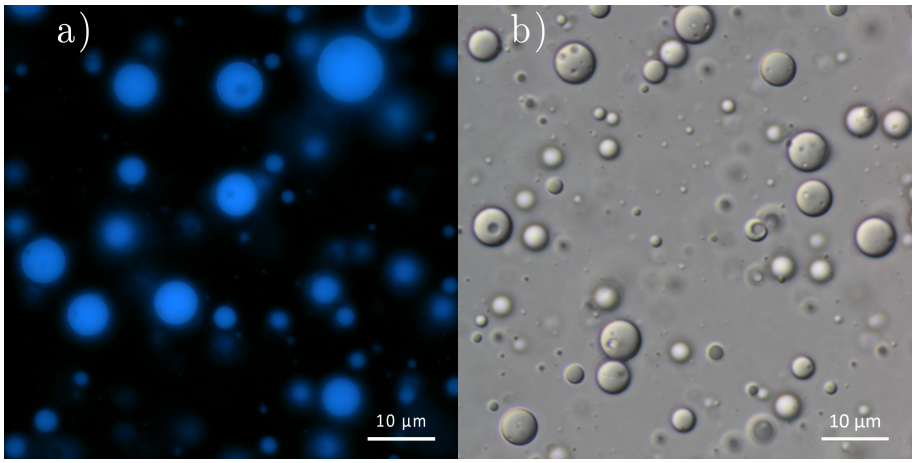

Figure 4.8: Ethyl cellulose microcapsules with ethyl linoleate cores and $m_s/m_c = 0.7$ imaged using a) fluorescence microscopy and b) optical microscopy.

Polycaprolactone

Polycaprolactone microcapsules were formulated with glyceryl trioctanoate as core material. As with ethyl cellulose microcapsules, no core-shell morphology could be seen. Rather, homogeneous spheres were observed. From the optical micrographs a rough and possibly porous surface was seen.

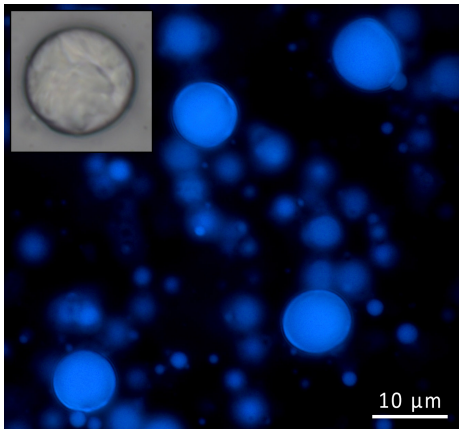

Figure 4.9: Fluorescence microscopy image of PCL microcapsules with glyceryl trioctanoate as the oil phase. In the inset, an optical micrograph of the rough surface structure of the capsules can be seen.

Several attempts to improve the spreading of the PCL coacervate phase were performed. To produce a smoother and less porous capsule surface, it was attempted to heat the formulated microcapsule suspension to 80 °C, above the melting point of the polymer, for a total of one hour followed by a slow cooling. However, no change in the capsule structure was seen. By altering the formulation procedure to use ethyl acetate rather than DCM it was attempted to perform the phase separation above the polymer melting point. The higher boiling point of ethyl acetate as compared to DCM allowed for the evaporation to be done at 70 °C. Rather than producing microcapsules on the scale of a few micrometers, a single *macrocapsule* of a few millimeters in size formed. No oily residue or free oil droplets could be observed which suggested that the oil either dissolved inside the PCL sphere or that it formed a matrix structure.

Poly(sebacic anhydride)

To obtain microcapsules from which a triggered release of the interior substance could be achieved, polyanhydrides were evaluated as shell materials. No core-shell structure was obtained for the microcapsules, but rather large birefringent fragments as visualized by polarized light microscopy in Figure 4.10. It was thought that the anhydride was highly crystalline which prevented the formation of core-shell particles. The polymer's high crystallinity may have affected the kinetic process of core-shell formation where the polymer had to spread around the oil core. Seeing as the polymer was not soluble in dichloromethane but rather in ethyl acetate at elevated temperatures, this could also suggest that some degradation had occurred during storage.

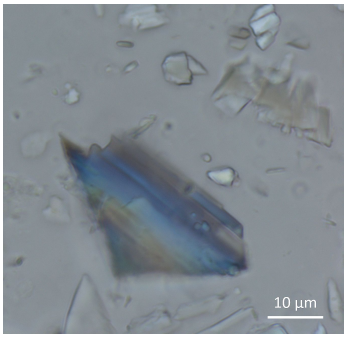

Figure 4.10: Polarized light microscopy image illustrating large birefringent fragments of poly(sebacic anhydride).

Size distribution functions were fitted to the ethyl cellulose and polycaprolactone microcapsules. The fitting parameters μ and σ is presented in Table 4.5. Although no clear core-shell structures were seen, the spheres were of similar size to PLGA microcapsules.

Table 4.5: Mean radii (μ) and standard deviations (σ) for the log-normal fittings from micrographs of ethyl cellulose and polycaprolactone microcapsules with glyceryl trioctanoate as core oil.

Shell material	Mean radius μ (µm)	Standard deviation σ (µm)
Ethyl cellulose	1.53 ± 0.07	0.65 ± 0.11
Polycaprolactone	1.48 ± 0.05	0.49 ± 0.07

4.2 Optimization for slow release

The formulated microcapsule systems had two drawbacks if a slow release was desired. Firstly, the active substance obtains a higher rate of diffusion in a liquid core as compared to a solid core which should increase the release rate. Secondly, the core was shifted to one side of the microcapsule. By having a centered core, the release rate could be decreased to give an even slower release.

4.2.1 Solid core for lower rate of diffusion

Microcapsules with ethyl stearate cores were formulated. The melting point of this oil phase was 36 °C, and it was subsequently solid at room temperature. Figure 4.11 illustrates the morphology of a core-shell particle with a solid core. Some of the cores appeared to have an uneven distribution of pyrene and they also affected the polarization of light used for the DIC-filter. This may be attributed to crystallinity of the solid fatty acid ester.

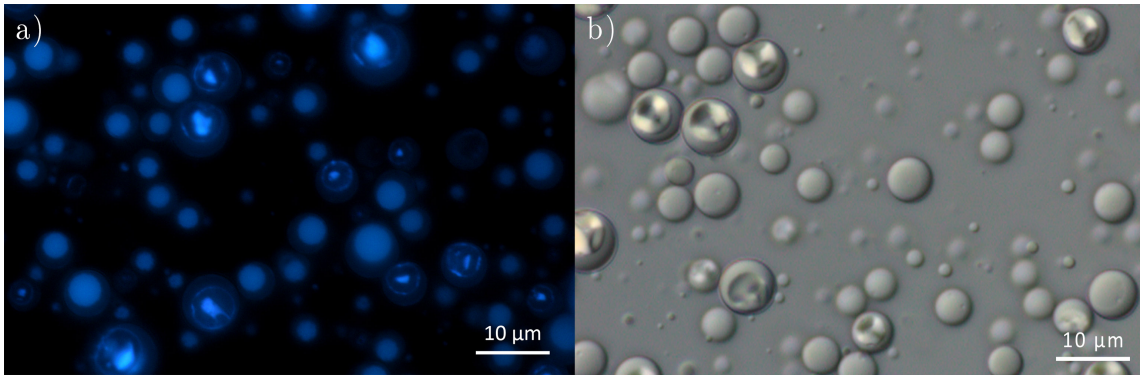

Figure 4.11: PLGA microcapsules with ethyl stearate cores visualized with a) fluorescence microscopy and b) optical microscopy using a DIC-filter.

4.2.2 Centering of the core

Attempts were made to produce microcapsules where the oil core was centered within the microcapsule. By adding hexadecane which is a more hydrophobic core, it was evaluated if the shifted core was due to unfavorable spreading conditions. No changes in capsule morphology could be observed, and the shifted cores were still observed. Spreading coefficients for hexadecane core - PLGA shell microcapsules are presented in Table 4.6. To investigate a possibly unfavorable interfacial spreading behavior, attempts with adding the oil-soluble nonionic surfactant Berol 533 at concentrations of 0.5 and 1 wt% of the core, respectively, were performed. This was done using PLGA of the higher molecular weight as these cores became more shifted. Rather than providing improved wetting, the oil-water interfacial tension was reduced to the point where an acorn morphology was formed, see Figure 4.12. This has been observed previously by Vincent and Loxley [8]. Furthermore heteroaggregates of polymer onto which multiple oil droplets were attached could be observed. Due to a lowered oil-water interfacial tension from the surfactant the energy loss in forming multiple oil droplets as compared to just one would be reduced. This may explain why these heteroaggregates formed, rather than a single acorn, when the surfactant was added.

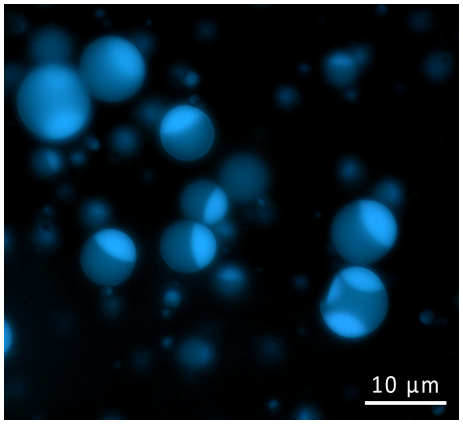

Figure 4.12: Fluorescence microscopy image of the acorn morphology obtained when adding Berol 533 to the core oil.

4.3 Theory of spreading kinetics

The process of phase separation can occur via an intermediate as illustrated in Figure 4.13. This is valid if the assumed final morphology is an oil-core polymer-shell particle and the polymer phase separates before the core oil. Depending on the three interfacial tensions $\gamma_{\mathrm{DCM}-w}$, γ_{pw} and $\gamma_{p-\mathrm{DCM}}$ different intermediates can form. For Figure 4.13a) the interfacial tension $\gamma_{\mathrm{DCM}-w}$ is greater than γ_{pw}. At the same time, the spreading conditions for core-shell formation are fulfilled even with DCM-oil as the core phase. To later form an oil core-polymer shell particle, the DCM has to diffuse out through the polymeric shell into the water phase from which it can evaporate. This has been observed by Atkin et al. in the case of aqueous core-polymer shell particles in a continuous oil phase with acetone as volatile solvent [52].

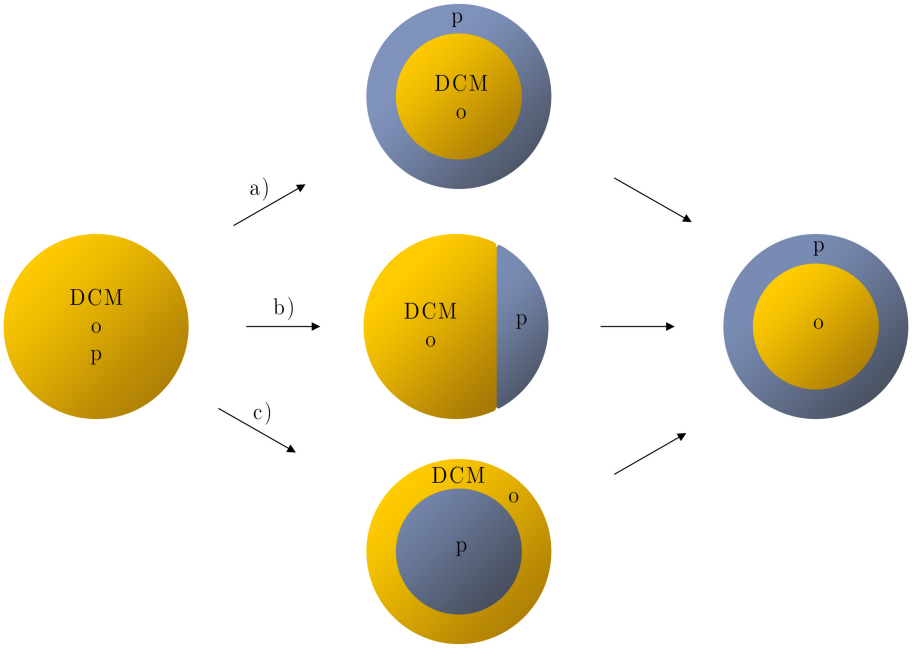

Figure 4.13: The kinetic process of internal phase separation. Three different intermediates are possible when going from a DCM droplet to a core-shell particle. In a) the polymer spreads around the DCM-oil droplet, in b) an acorn structure is formed between DCM-oil and polymer and in c) the DCM-oil spreads around the polymer.

If instead the interfacial tension $\gamma_{\text{DCM-w}}$ is not sufficiently high, or γ_{pw} is not sufficiently low, an acorn particle would form as in Figure 4.13b). Interfacial tensions such that $\gamma_{\text{DCM-w}} < \gamma_{\text{pw}}$ would form an inverted particle where the DCM-oil completely engulfs a polymeric sphere. The two routes in Figure 4.13b) and c) consequently present a more complex phase separation behavior that can affect the quality of the microcapsules.

An even more favorable intermediate would be available if the core oil phase separated before the polymer. By enabling this, an inverted form of the intermediate in Figure 4.13c) would be present where a DCM-polymer mixture would spread around an oil core. As no DCM has to leach out through a solidified polymer shell, the porosity in the shell theoretically becomes lower. This can in turn lead to a slower release rate [47].

Due to the higher solubility of the core oil in DCM as compared to the polymers, it is hypothesized that this prevented the desired spreading of the polymer around the core. Given that the polymer phase separated before the oil, a three-phase system consisting of water, polymer and DCM-oil would be observed at some point during the evaporation process of DCM. By measuring the interfacial tension between 1 wt% PVA in water and DCM, and fitting the experimental data to Equation 3.2 the value of $\gamma_{\text{DCM-w}}$ was found to be 8.34 mN/m. It was consequently assumed that the DCM-oil coacervate was pure DCM. All the fitted parameters and a plot of the experimental data is presented in Table A.2 and Figure A.1 in the appendix. Since

DCM dissolves PLGA, no contact angle of DCM on PLGA could be determined and it was hence assumed to be 0. From Equation 2.8 the PLGA-DCM interfacial tension could then be calculated.

Knowing the three previously mentioned interfacial tensions, spreading coefficients for the simplified three-phase system consisting of 1 wt% PVA in water - DCM - PLGA, Figure 4.13, could be calculated and is presented in Table 4.6. In reality, there would be DCM present in the polymer phase during coacervation and likewise there would be small amounts of PLGA and core oil present in the DCM-phase. Due to the experimental difficulty in measuring this, it was consequently neglected. The predicted morphology for this system was acorn particles, as illustrated schematically in Figure 4.13. This suggested that the acorn particle would have to change its morphology into a core-shell particle as the DCM evaporated and only the alkane or fatty acid ester core remained. The small amounts of DCM left at the time of this morphology change would make it hard for the polymer to fully spread around the oil phase. This may be an explanation to why the shifted oil cores were observed in the formulated core-shell particles. The more shifted core obtained with higher molecular weight PLGA was also explained by this model. A higher molecular weight of the shell would give it a higher viscosity and thus less mobility to transition from the intermediate acorn to the final core-shell structure. It is worth noting that there is no thermodynamical driving force for centering the core. As long as there is a polymer film engulfing the entire oil droplet, the thermodynamics does not promote a centered core over a shifted core.

Table 4.6: Interfacial tensions and calculated spreading coefficients for two of the investigated systems. The theoretical intermediate system where the oil phase consists of DCM is also included. Indices o and p are the oil and polymer phases respectively, and w is the water phase containing 1 wt% PVA. Interfacial tensions are presented in mN/m.

							Morphology	
Oil phase	γ_{ow}	γ_{po}	γ_{pw}	S_o	S_w	S_p	Predicted	Observed
Hexadecane	21.24	6.73	11.05	-16.92	-25.56	3.47	Core-shell	Core-shell
DCM	8.34	6.37	11.05	-3.66	-13.02	-9.08	Acorn	-
Perfluoro-octane	27.73	19.16	11.05	-35.84	-19.62	-2.47	Acorn	Acorn

To test whether this hypothesis was true, perfluorooctane that phase separated before the polymer was chosen as the oil phase. By having an oil phase that separates before the polymer, the intermediates in Figure 4.13 would be avoided. Instead, an intermediate where a DCM-polymer mixture spreads around the phase separated droplet would form. From a kinetic point of view this was the most favorable intermediate. The determination of the spreading coefficients for this system in Table 4.6 showed that the interfacial tension between polymer and oil became too high to enable the formation of perfluorocarbon core-PLGA shell particles. Rather, acorn particles were predicted and this was also observed when these particles were formulated. This is seen in Figure 4.14. Due to the low solubility of any regular dye in the fluorinated alkane, it was not possible to visualize the morphology by

fluorescence microscopy. Rather than distributing in the core, the added pyrene distributed selectively in the shell.

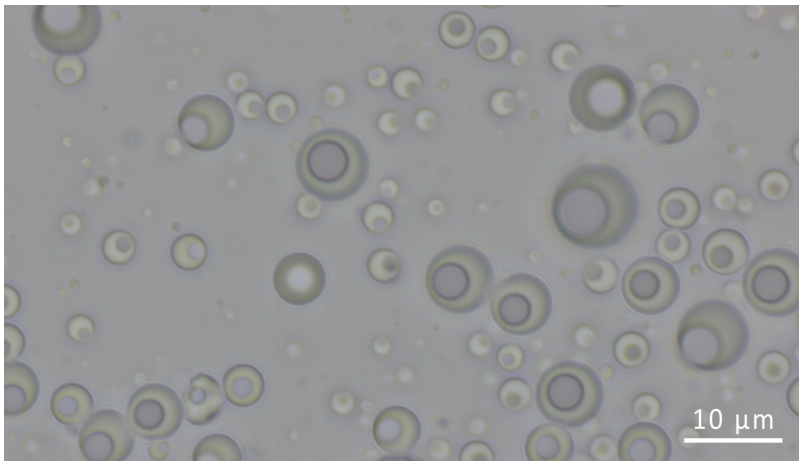

Figure 4.14: Acorn particles observed for PLGA and perfluorooctane.

Pisani et al. did successfully produce fluorinated alkane core-PLGA shell particles following the internal phase separation route by replacing PVA in the water phase by sodium cholate [53]. By using confocal scanning laser microscopy the stained polymer shell was visualized. This way, the core was seen to be centered within the capsule. This strengthened the theory that the shifted core was a result from the unfavorable intermediate where solidifying PLGA had to spread around a DCM-oil droplet.

To promote the intermediate in Figure 4.13a), the polymer-water interfacial tension has to be lowered and the DCM-water interfacial tension had to be increased. By using PVA as dispersant in the water phase, the interfacial tension of DCM against water is reduced from 28 mN/m for pure water to 8 mN/m. By formulating PMMA-microcapsules with a poly(methyl methacrylate-b-sodium methacrylate) (PMMA-b-PMANa) block-copolymer at 0.4 wt% in the water phase as dispersant, an exceptionally low polymer-water interfacial tension can be obtained from the entanglements of the PMMA block in the shell [11]. It was therefore attempted to produce such microcapsules. The dispersant was found to have degraded over time and did hence not produce well-dispersed core-shell particles, but rather particles that were slightly flocculated. Furthermore, no centering of the core could be observed, which can be attributed to a higher polymer-water interfacial tension due to the degradation of the dispersant.

4.4 Controlled release of pyrene

The fractional release from PLGA microcapsule formulations with altered core substances is presented in Figure 4.15. An extraordinarily slow release of the active

was observed for all of the systems, as compared to microcapsule systems in the literature [47, 54]. Given the hydrophobicity of pyrene and the hydrophilicity of PLGA, this was expected. The equilibrium constant for pyrene between the release medium and the capsule itself was seen to change between the oil phases, with ethyl linoleate being separated from the rest of the core oils.

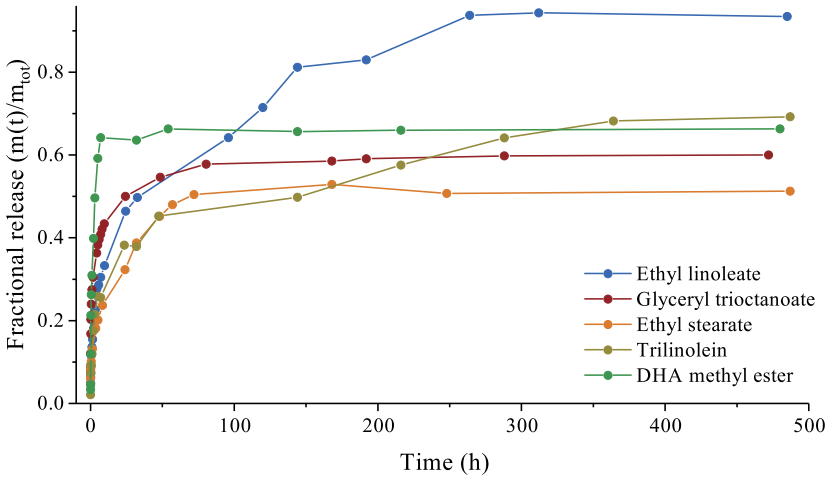

Figure 4.15: Fractional release from PLGA microcapsules with $m_s/m_c = 3$ as a function of time.

To visualize the finer details in the initial part of the release curve, the release was plotted on a logarithmic time scale as seen in Figure 4.16. The release from DHA-containing microcapsules was significantly faster as compared to other core oils. This may be attributed to the fact that the core oil oxidized at such a rapid rate. By adding antioxidants to the release system, a slower release may have been observed. Furthermore, only a minor difference in release could be observed from microcapsules with the solid ethyl stearate as core material. Previous studies have shown a significantly slower release from microcapsules with solid cores as compared to liquid cores [54]. This suggested that the rate determining diffusion was the diffusion through the shell and not diffusion inside the core, even when a solid core was used.

The comparison between release from PCL microcapsules with two different molecular weights of PLGA is presented in Figure 4.17. PCL microcapsules reached an equilibrium with the released active substance within minutes, and the same was observed for PLGA with the higher molecular weight of 100 kDa. No changes in the capsule structure could be observed for the PCL capsules, but capsules made from PLGA with the molecular weight 100 kDa were seen to break when added to the release bath, likely due to the thin shell present on one side of the capsule. The release profile from PCL microcapsules further strengthened the theory that a matrix structure was formed inside the spheres. By not having a solid polymeric shell encapsulating the oil, it was freely exposed to the surrounding release medium which gave a virtually instant release of pyrene.

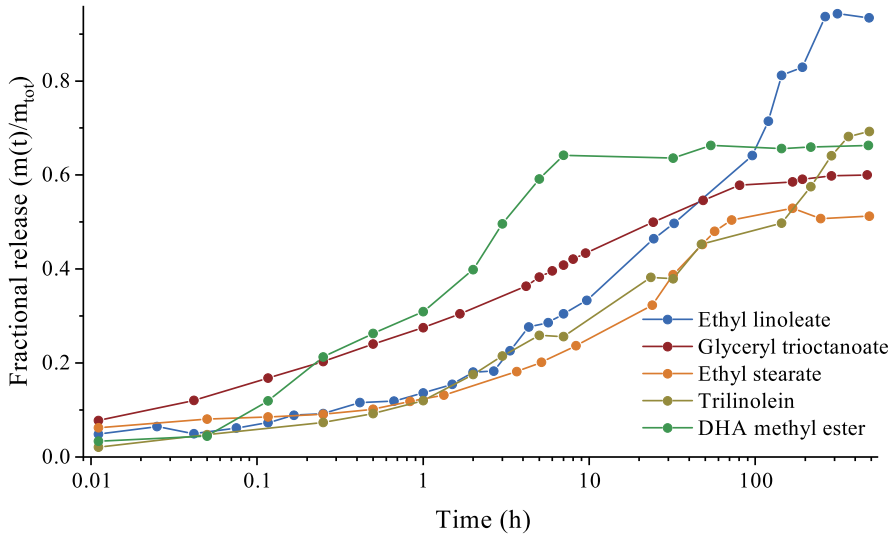

Figure 4.16: Fractional release from PLGA microcapsules with $m_s/m_c = 3$ as a function of time.

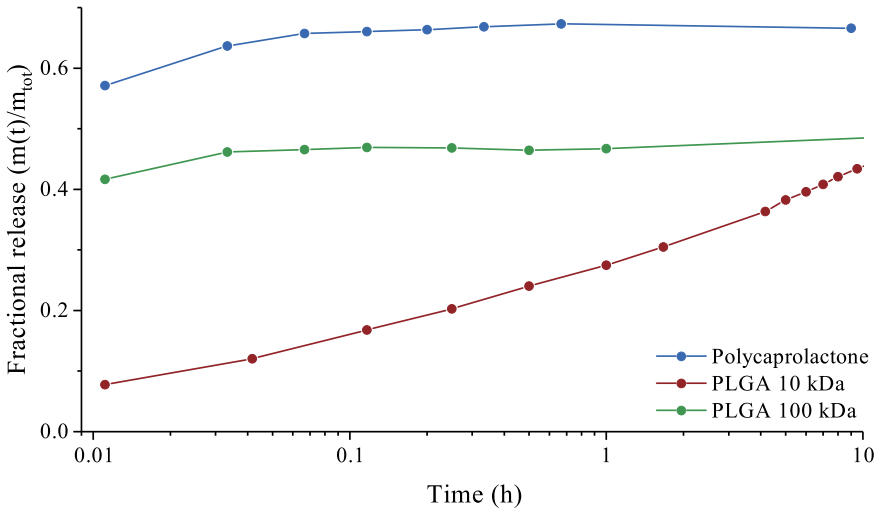

Figure 4.17: Fractional release as a function of time for PCL and two molecular weights of PLGA. The core oil was glyceryl trioctanoate for all measurements and $m_s/m_c = 3$.

4.4.1 Effect of microcapsule stability on the release

Although an increasing amount of free oil droplets could be observed over time in the suspension as the microcapsules were stored, it was desired to know to what extent this affected the release profile from the microcapsules. In Figure 4.18 the fractional release from microcapsules with an ethyl linoleate core and $m_s/m_c = 3$ is presented, both directly after formulation and after one week of storage under gentle

magnetic stirring. A large relative burst release of $0.37 \cdot m_{\text{tot}}$ could be observed. For the freshly prepared sample, the fractional burst release was close to zero. The burst release was likely occurring from the free oil droplets as there was no polymer shell to act as a diffusion barrier around these reservoirs. For the second part of the release from the stored samples, pyrene dissolved in the empty polymeric shells and the still intact core-shell particles was released. The slope of the two release profiles was similar, only separated by the initial burst release for the aged sample. This suggested that the capsules that still were intact after one week released the actives at the same rate as freshly prepared capsules.

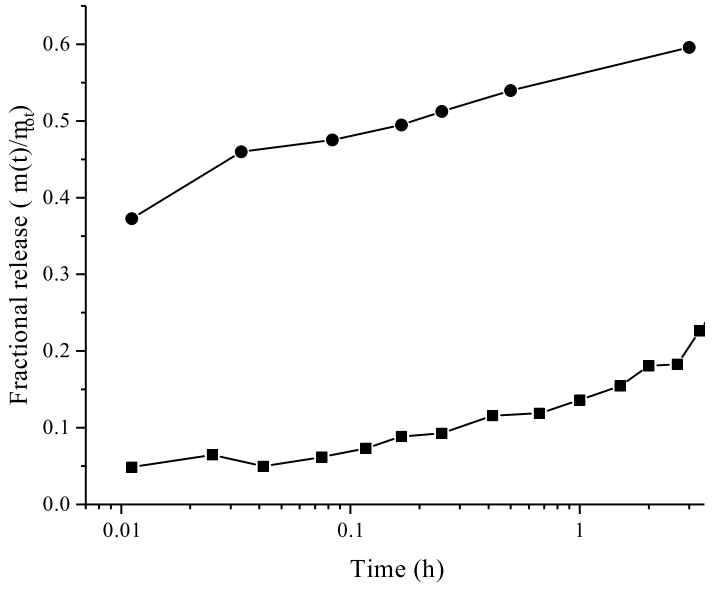

Figure 4.18: Fractional release from PLGA microcapsules with ethyl linoleate cores prepared freshly before release measurements (■) and after one week of storage (●).

5

Conclusion

Through encapsulation of actives into microcapsules, their release can be prolonged and controlled. In this work, biocompatible and biodegradable core-shell particles have been formulated. It has been shown that there is a relatively large freedom in the choice of core substance when PLGA is used as shell material. Triglycerides with C8:0 fatty acids have been successfully encapsulated as well as methyl esters of C22:6 fatty acids. By determining spreading coefficients for the PLGA microcapsules, a theoretical foundation has been laid to explain the observed capsule morphologies. From all of the investigated microcapsules, a slow release of pyrene was observed. The major rate-determining barrier for the release was therefore the PLGA shell. Although pyrene is a good model compound in terms of its physicochemical properties, it is worth noting that active substances often are semi-hydrophobic and surface active which can affect interfacial tensions and thereby the observed capsule morphologies significantly.

From the prepared size distributions it has been shown that an unbiased determination of the size distribution is possible by particle counting of optical microscopy images by comparing the results with results from light scattering. There is also a reproducibility in the formulation methodology as similar sizes were obtained for all microcapsules.

The library of biodegradable and biocompatible shell materials available for producing core-shell particles requires further investigation. The aliphatic anhydride poly(sebacic anhydride) did not produce any spherical structures. It would therefore be interesting to further explore previously investigated anhydride structures with aromatic segments to produce a biodegradable microcapsule with triggered release [50]. No clear core-shell structures were seen for ethyl cellulose and polycaprolactone microcapsules. Analyzing the cross-sections of the spheres by scanning electron microscopy would further elucidate the internal morphology.

To further understand the kinetics of core-shell formation, prepared emulsions can be monitored as the volatile solvent evaporates. This would verify the validity of the presented model of how a core-shell particle is formed with a possible intermediate morphology. By further investigating the use of specifically engineered block copolymers to reduce the polymer-water interfacial tension and increase DCM-water

interfacial tension, the intermediates could be altered. A more hydrophilic polymer, such as PLGA with a different ratio between the monomers, may also have more beneficial interfacial tensions.

Finally, it would be interesting to evaluate the release of active antibacterial quaternary ammonium compounds from core-shell particles. Incorporation of core-shell particles into cellulose fibers would also provide useful information for future applications.

Bibliography

[1] World Health Organization et al. *Global report on diabetes*. World Health Organization, 2016.

[2] Garth A. James et al. "Biofilms in chronic wounds". In: *Wound Repair and Regeneration* 16.1 (2008), pp. 37–44.

[3] World Union of Wound Healing Societies. *Management of biofilms*. 2016.

[4] R. Cammack et al. *Oxford Dictionary of Biochemistry and Molecular Biology*. 2nd ed. Oxford University Press, 2006. ISBN: 978-0-19-852917-0.

[5] Markus Andersson Trojer et al. "Encapsulation of actives for sustained release". In: *Phys. Chem. Chem. Phys.* 15 (41 2013), pp. 17727–17741.

[6] Jeong-Sook Cho, Aehwa Kwon, and Chang-Gi Cho. "Microencapsulation of octadecane as a phase-change material by interfacial polymerization in an emulsion system". In: *Colloid and Polymer Science* 280.3 (Mar. 2002), pp. 260–266.

[7] Claire S. Peyratout and Lars Dähne. "Tailor-Made Polyelectrolyte Microcapsules: From Multilayers to Smart Containers". In: *Angewandte Chemie International Edition* 43.29 (2004), pp. 3762–3783.

[8] Andrew Loxley and Brian Vincent. "Preparation of Poly(methylmethacrylate) Microcapsules with Liquid Cores". In: *Journal of Colloid and Interface Science* 208.1 (1998), pp. 49–62. ISSN: 0021-9797. DOI: 10.1006/jcis.1998.5698.

[9] Shijia Tang et al. "Low-Ceiling-Temperature Polymer Microcapsules with Hydrophobic Payloads via Rapid Emulsion-Solvent Evaporation". In: *ACS Applied Materials & Interfaces* 9.23 (2017), pp. 20115–20123.

[10] CJ Van Oss, RJ Good, and MK Chaudhury. "Additive and nonadditive surface tension components and the interpretation of contact angles". In: *Langmuir* 4.4 (1988), pp. 884–891.

[11] Markus Andersson Trojer et al. "Charged microcapsules for controlled release of hydrophobic actives. Part I: encapsulation methodology and interfacial properties". In: *Soft Matter* 9 (5 2013), pp. 1468–1477.

[12] Eric Stauffer, Julia A. Dolan, and Reta Newman. *Fire Debris Analysis*. Elsevier, 2008. ISBN: 978-0-12-663971-1.

[13] Richard D. O'Brien, Walter E. Farr, and Peter J. Wan. *Introduction to Fats and Oils Technology (2nd Edition)*. AOCS Press, 2000. ISBN: 978-1-893997-13-4.

[14] Ashok Pandey et al. *Industrial Biorefineries and White Biotechnology*. Elsevier, 2015. ISBN: 978-0-444-63453-5.

[15] Ernst Krendlinger et al. “Waxes”. In: *Ullmann’s Encyclopedia of Industrial Chemistry*. 2015, pp. 16–17.

[16] Fangrui Ma and Milford A Hanna. “Biodiesel production: a review”. In: *Bioresource Technology* 70.1 (1999), pp. 1–15.

[17] Zvi Cohen and Colin Ratledge. *Single Cell Oils - Microbial and Algal Oils: Significance of docosahexaenoic acid*. 2nd ed. AOCS Press, 2010.

[18] Rebecca Wall et al. “Fatty acids from fish: the anti-inflammatory potential of long-chain omega-3 fatty acids”. In: *Nutrition reviews* 68.5 (2010), pp. 280–289.

[19] Harold W. Gardner. “Oxygen radical chemistry of polyunsaturated fatty acids”. In: *Free Radical Biology and Medicine* 7.1 (1989), pp. 65–86. ISSN: 0891-5849.

[20] Edwin N Frankel. “Lipid oxidation: mechanisms, products and biological significance”. In: *Journal of the American Oil Chemists’ Society* 61.12 (1984), pp. 1908–1917.

[21] Albert W. Girotti. “Mechanisms of lipid peroxidation”. In: *Journal of Free Radicals in Biology & Medicine* 1.2 (1985), pp. 87–95. ISSN: 0748-5514.

[22] Stephen J. Blanksby and G. Barney Ellison. “Bond Dissociation Energies of Organic Molecules”. In: *Accounts of Chemical Research* 36.4 (2003), pp. 255–263.

[23] Y. Serfert, S. Drusch, and K. Schwarz. “Chemical stabilisation of oils rich in long-chain polyunsaturated fatty acids during homogenisation, microencapsulation and storage”. In: *Food Chemistry* 113.4 (2009), pp. 1106–1112. ISSN: 0308-8146.

[24] A. L. Branen. “Toxicology and biochemistry of butylated hydroxyanisole and butylated hydroxytoluene”. In: *Journal of the American Oil Chemists’ Society* 52.2 (Feb. 1975), p. 59.

[25] Piergiorgio Gentile et al. “An overview of poly (lactic-co-glycolic) acid (PLGA)-based biomaterials for bone tissue engineering”. In: *International journal of molecular sciences* 15.3 (2014), pp. 3640–3659.

[26] James M Anderson and Matthew S Shive. “Biodegradation and biocompatibility of PLA and PLGA microspheres”. In: *Advanced Drug Delivery Reviews* 28.1 (1997), pp. 5–24. ISSN: 0169-409X.

[27] N. Faisant et al. “Effects of the type of release medium on drug release from PLGA-based microparticles: Experiment and theory”. In: *International Journal of Pharmaceutics* 314.2 (2006), pp. 189–197.

[28] Banu S. Zolnik and Diane J. Burgess. “Effect of acidic pH on PLGA microsphere degradation and release”. In: *Journal of Controlled Release* 122.3 (2007). Proceedings of the Thirteenth International Symposium on Recent Advances in Drug Delivery Systems, pp. 338–344.

[29] Maria Ann Woodruff and Dietmar Werner Hutmacher. “The return of a forgotten polymer—Polycaprolactone in the 21st century”. In: *Progress in Polymer Science* 35.10 (2010), pp. 1217–1256.

[30] Dietmar W. Hutmacher. “Scaffolds in tissue engineering bone and cartilage”. In: *Biomaterials* 21.24 (2000), pp. 2529–2543.

[31] K. W. Leong, B. C. Brott, and R. Langer. “Bioerodible polyanhydrides as drug-carrier matrices. I: Characterization, degradation, and release characteristics”. In: *Journal of Biomedical Materials Research* 19.8 (1985), pp. 941–955.

[32] Lars Alexander Schneider et al. “Influence of pH on wound-healing: a new perspective for wound-therapy?” In: *Archives of Dermatological Research* 298.9 (2007), pp. 413–420.

[33] Edith Mathiowitz et al. “Morphological characterization of bioerodible polymers. 1. Crystallinity of polyanhydride copolymers”. In: *Macromolecules* 23.13 (1990), pp. 3212–3218.

[34] U. Edlund and A. -C. Albertsson. “Degradable Polymer Microspheres for Controlled Drug Delivery”. In: *Degradable Aliphatic Polyesters*. Berlin, Heidelberg: Springer, 2002, pp. 67–112. ISBN: 978-3-540-45734-3.

[35] Ann-Christine Albertsson and Maria Eklund. “Influence of molecular structure on the degradation mechanism of degradable polymers: In vitro degradation of poly(trimethylene carbonate), poly(trimethylene carbonate-co-caprolactone), and poly(adipic anhydride)”. In: *Journal of Applied Polymer Science* 57.1 (1995), pp. 87–103.

[36] R.C. Rowe. “Molecular weight dependence of the properties of ethyl cellulose and hydroxypropyl methylcellulose films”. In: *International Journal of Pharmaceutics* 88.1 (1992), pp. 405–408.

[37] Julide Akbuğa. “Furosemide-loaded ethyl cellulose microspheres prepared by spherical crystallization technique: Morphology and release characteristics”. In: *International Journal of Pharmaceutics* 76.3 (1991), pp. 193–198.

[38] S.M. Mirabedini, I. Dutil, and R.R. Farnood. “Preparation and characterization of ethyl cellulose-based core–shell microcapsules containing plant oils”. In: *Colloids and Surfaces A: Physicochemical and Engineering Aspects* 394 (2012), pp. 74–84.

[39] Thamara Laredo, Shai Barbut, and Alejandro G. Marangoni. “Molecular interactions of polymer oleogelation”. In: *Soft Matter* 7 (6 2011), pp. 2734–2743.

[40] Bernard Valeur and Mário Nuno Berberan-Santos. *Molecular fluorescence: principles and applications*. 2nd ed. John Wiley & Sons, 2013.

[41] Mansoor M. Amiji. “Pyrene fluorescence study of chitosan self-association in aqueous solution”. In: *Carbohydrate Polymers* 26.3 (1995), pp. 211–213. ISSN: 0144-8617.

[42] J. B. Birks. “Excimers”. In: *Reports on Progress in Physics* 38.8 (1975), pp. 903–974.

[43] Joseph R Lakowicz. *Principles of fluorescence spectroscopy*. Springer Science & Business Media, 2013.

[44] K.J Packer and C Rees. “Pulsed NMR studies of restricted diffusion. I. Droplet size distributions in emulsions”. In: *Journal of Colloid and Interface Science* 40.2 (1972), pp. 206–218. ISSN: 0021-9797.

[45] AP Altshuller and HE Everson. “The solubility of ethyl acetate in water”. In: *Journal of the American Chemical Society* 75.7 (1953), pp. 1727–1727.

[46] Lars Nordstierna, Alireza Movahedi, and Magnus Nydén. “New Route for Microcapsule Synthesis”. In: *Journal of Dispersion Science and Technology* 32.3 (2011), pp. 310–311.

[47] Jonatan Bergek et al. “Controlled release of microencapsulated 2-n-octyl-4-isothiazolin-3-one from coatings: Effect of microscopic and macroscopic pores”. In: *Colloids and Surfaces A: Physicochemical and Engineering Aspects* 458 (2014), pp. 155–167.

[48] Xi Yuan Hua and Milton J Rosen. “Dynamic surface tension of aqueous surfactant solutions: I. Basic paremeters”. In: *Journal of Colloid and Interface Science* 124.2 (1988), pp. 652–659. ISSN: 0021-9797.

[49] Jonatan Bergek. *Evaluation of Biocide Release from Modified Microcapsules*. Department of Chemistry and Chemical Engineering, Chalmers University of Technology, 2017.

[50] Gustav Eriksson. “Microencapsulation of actives for the healthcare of tomorrow. Formulation of core-shell microcapsules using biocompatible materials for extended and triggered release of actives”. Master’s thesis. Department of Chemistry and Chemical Engineering, Chalmers University of Technology, 2018.

[51] Markus Andersson Trojer et al. “Use of microcapsules as controlled release devices for coatings”. In: *Advances in Colloid and Interface Science* 222 (2015), pp. 18–43.

[52] Rob Atkin et al. “Preparation of Aqueous Core/Polymer Shell Microcapsules by Internal Phase Separation”. In: *Macromolecules* 37.21 (2004), pp. 7979–7985.

[53] E. Pisani et al. “Polymeric Nano/Microcapsules of Liquid Perfluorocarbons for Ultrasonic Imaging: Physical Characterization”. In: *Langmuir* 22.9 (2006), pp. 4397–4402.

[54] Mariam Masuda. *Microencapsulation of pesticides for controlling release from coatings*. Chalmers University of Technology, 2011.

A

Appendix 1

Table A.1: Solubility of pyrene in tested core oils.

Compound	Solubility [% (w/w)]
Ethyl linoleate	8*
Olive oil	5
Sunflower oil	6

A.1 Optical tensiometry

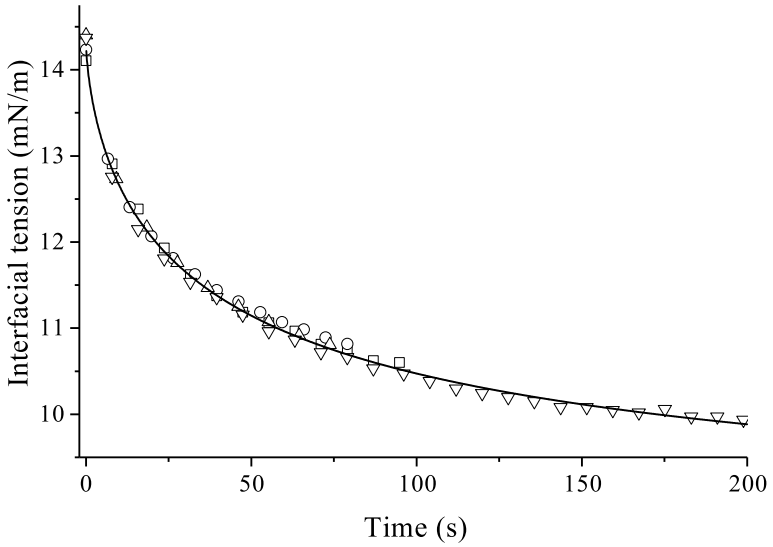

Figure A.1: Dynamic interfacial tension of DCM against 1 wt% PVA in water. Four replicates of the measurements were done.

*Gustav Eriksson. "Microencapsulation of actives for the healthcare of tomorrow. Formulation of core-shell microcapsules using biocompatible materials for extended and triggered release of actives". Master's thesis. Department of Chemistry and Chemical Engineering, Chalmers University of Technology, 2018.

Table A.2: Fitted parameters to equation 3.2 for the interfacial tension between 1 wt% PVA in water against DCM.

Interface	γ_e (mN/m)	γ_0 (mN/m)	τ (s)	n
1 wt% PVA - DCM	8.34 ± 0.18	14.32 ± 0.06	41.56 ± 3.51	0.67 ± 0.03

Table A.3: Surface tension components of the test liquids used for surface characterization of PLGA along with their contact angles on PLGA. Surface tensions are presented in mN/m and contact angles (θ) in degrees.

Test liquid	γ_L^{tot}	γ_L^{LW}	γ_L^+	γ_L^-	θ
Diiodomethane	50.8	50.8	0	0	39.4
Glycerol	63.4	40.6	3.9	57.4	75.7
Hexadecane	27.5	27.5	0	0	< 5
Water	72.8	21.8	25.5	25.5	69.3
Ethyl linoleate	22.8				< 5
Glyceryl tributyrate	28.8				< 5
Perfluorooctane	13.7				< 5
1 wt% PVA in water	60.6				68.9
Dichloromethane	26.5				